



---

LARGE SYNOPTIC SURVEY TELESCOPE

---

**Large Synoptic Survey Telescope (LSST)**

**LSST Crowded Fields photometry**

**K. Suberlak, C. Slater, Ž. Ivezić**

**LSST-2017**

**Latest Revision: 2018-03-06**

revision: TBD  
status: draft

## Abstract

A report on the performance of current LSST Stack pipelines in crowded stellar fields. We use the DECAPS data to provide the photometry and astrometry quality assurance metrics. The mean completeness of LSST detections compared to DECAPS between 18-20 mag is at the level of 82% for regions with 200 000 sources per sq. deg. (top 10 % density). For the same density, the completeness drops to 50% at 21.2 mag.

The systematic offset in photometry (the difference between the median photometric uncertainty and the measure of internal photometric repeatability) at 21 mag for the density of 200 000 sources per sq.deg. is 0.06 mag.

The LSST photometry is consistent with DECAPS at the 1% level, as long as the density is not above 35 000 sources per sq. deg.

The spread of astrometric repeatability is at the level of 10 miliarcsec, with no significant dependence on stellar crowdedness, which is better than the investigated DECAPS astrometry thanks to the LSST pipeline being tied to GAIA astrometry.



## Change Record

Version	Date	Description	Owner name
1	2017-07-16	First draft.	Krzysztof Suberlak
2	2017-10-19	Updated outline.	Krzysztof Suberlak
2	2018-01-25	Major revision.	Krzysztof Suberlak
2	2018-03-04	Reorganized the draft.	Krzysztof Suberlak

## Contents

<b>1</b>	<b>Introduction</b>	<b>1</b>
<b>2</b>	<b>Identifying density regions</b>	<b>2</b>
<b>3</b>	<b>DECam Plane Survey</b>	<b>3</b>
<b>4</b>	<b>LSST Processing of DECAPS data</b>	<b>7</b>
4.1	Cleaning DECAPS catalog, comparison to LSST pixel mask . . . . .	9
4.2	Cleaning LSST catalog . . . . .	10
<b>5</b>	<b>Metrics</b>	<b>16</b>
5.1	Completeness . . . . .	16
5.2	Photometry . . . . .	17
<b>6</b>	<b>Astrometry</b>	<b>26</b>
<b>7</b>	<b>Future work</b>	<b>28</b>
7.1	LSST Processing of StarFast Simulated Sky . . . . .	33
7.2	Other LSST-DECAPS tests: w-color . . . . .	33

## 1 Introduction

We report on the performance of the Large Scale Synoptic Telescope (LSST) science pipelines<sup>1</sup>, also known as 'the LSST stack', in stellar fields of varying levels of crowdedness.

The LSST will sample every night on average over 500 regions in the sky , delivering terabytes of raw data in need of processing: photometric and astrometric calibration, to deliver a calibrated exposure image, as well as a source catalog, among other image products<sup>2</sup> [7].

The survey sky is composed of regions very diverse in terms of stellar density, or crowdedness. Assuming the single-visit depth., the stellar density ranges from high density low-galactic latitude regions that have tens of millions of sources per square degree, to low-density regions towards the Galactic poles with less than thousand sources per square degree.

Deblending and successful photometry is an inherent part of any astronomical data processing pipeline. There exists a body of research answering questions that are specific to crowded stellar fields, eg. how many beams do we need per source (see [2]), or how the crowded fields photometry can be approached in the era of large telescopes [8] Other studies involved eg. HyperSuprime CAM pipeline ( developed in parallel with the LSST Stack), recognizing that the deeper the survey, the higher the stellar densities encountered, and the onset of blurring the boundaries between deblending, measurement, and detection [1].

In this report we compare the 'out-of-the-box' LSST Stack tools, in particular processCcd.py, to the DECAm [Galactic] Plane Survey (DECAPS) catalogs based on the DECAPS pipeline developed by Schlafly et al. [9]. First we use the LSST Metrics Analysis Framework Galfast simulation of the night sky find regions representing various stellar densities - see Sec. 2. Then we query the DECAPS image database for images that were taken at exposures and filters that reach similar depth to the LSST single-visit depth (Sec. 3). We select few DECAPS exposures at each density level, and process with LSST Stack tools (Sec. 4). In Sec. 5 we compare the results of LSST processing and the DECAPS single-epoch catalogs, and develop the quality metrics. Finally in Sec. 7 we make recommendations for future work.

<sup>1</sup><https://pipelines.lsst.io>

<sup>2</sup><http://ls.st/LSE-163>

## 2 Identifying density regions

To identify regions representing different stellar densities we use the LSST Metrics Analysis Framework<sup>3</sup> simulated stellar density map prepared by P. Yoachim and L. Jones with Galfast<sup>4</sup>

The resulting dataset `starDensity_r_nside_64.npz` contains 64 magnitude bins between 15 and 28 mag, with each bin containing the cumulative count of sources per square degree up to and including a given magnitude, with the entire sky divided into 49152 healpixels<sup>5</sup>. Each healpixel / magnitude bin contains information about the cumulative count of stars per square degree - see Fig. 1.

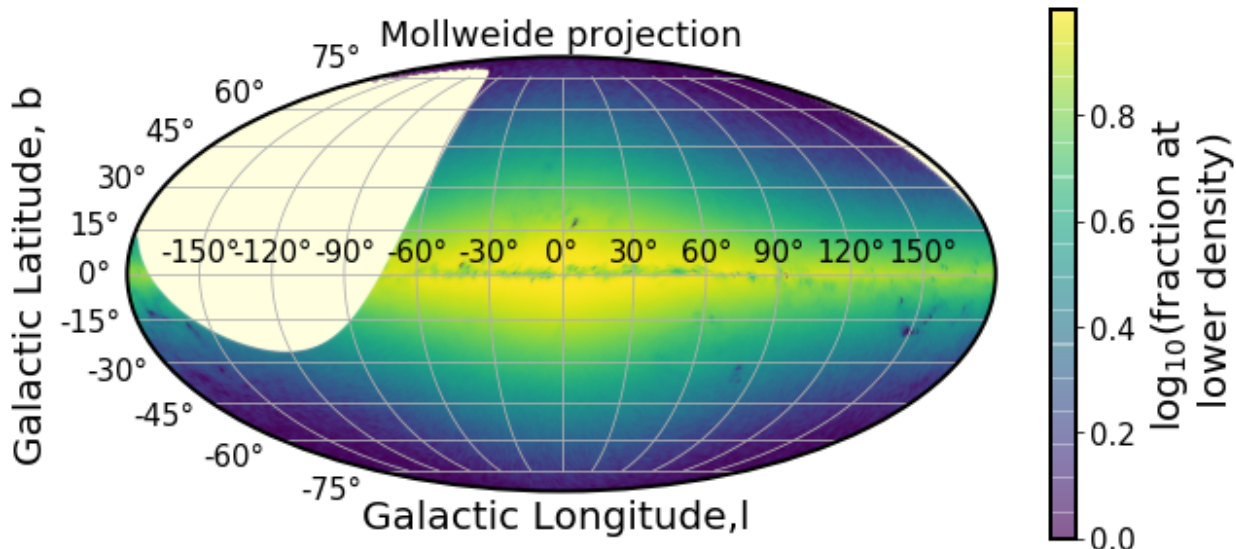


FIGURE 1: Galfast healpixels plotted in galactic coordinates in Mollweide projection. The brightest regions correspond to highest stellar densities. The missing part in the higher declination is the part of the sky above  $\delta > 40^\circ$ , which is not observable from the southern location of Cerro Pachón.

To match the LSST single-visit depth, we select magnitude bins smaller than  $r=24.5$ . For each healpixel we calculate the number of pixels that have a higher stellar count. Since each healpixel has an equal area, the fraction of pixel number above a certain threshold corresponds to the fraction of sky area above given density limit. Fig. 2 illustrates how we define percentiles of stellar densities, so that eg. 'top 1%' density means that only 1 in 100 pixels has

<sup>3</sup><https://www.lsst.org/scientists/simulations/maf>, and [https://github.com/lsst/sims\\_maf](https://github.com/lsst/sims_maf)

<sup>4</sup>[sims\\_maf/python/lsst/sims/maf/maps/createStarDensitymap.py](https://github.com/lsst/sims_maf/blob/python/lsst/sims/maf/maps/createStarDensitymap.py)

<sup>5</sup><http://healpix.sourceforge.net>

a higher density than a given pixel, and ‘top 10%’ means that ‘10 %’ of pixels in the considered simulation of the sky.

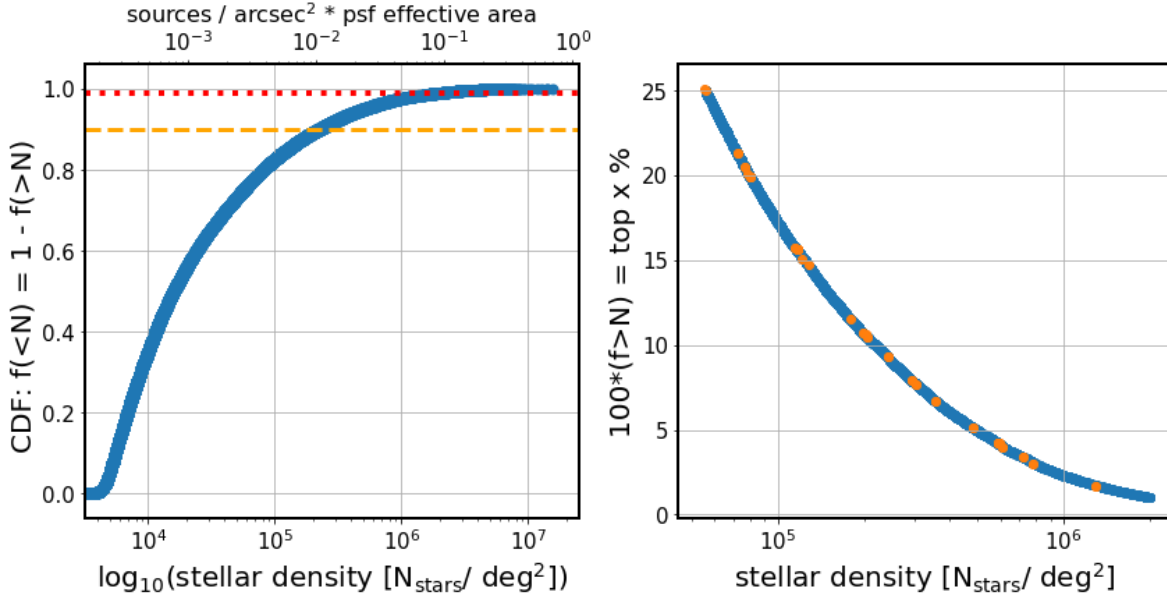


FIGURE 2: Using the Galfast sky simulation to choose DECAPS fields sampling different density regions. The left panel shows the stellar density as a function of the fraction of the sky at smaller density. It is equivalent to the cumulative distribution function. Given the stellar density per simulated healpixel, we count the number of healpixels at greater density. Normalized to the number of pixels, given their equal area, it corresponds to the fraction of the sky at greater stellar density. Horizontal dashed lines illustrate selecting pixels at top 1% or 10% density. The right panel focuses on the 1-CDF, converted to %, between 1 and 25%. It implies that according to the simulation, the density of 200 000 stars per sq.deg. corresponds to 5% of the sky, and only 1% of the sky has more than  $10^6$  stars per sq.deg. The upper axis represents the dimensionless density parameter  $N_{\text{beam}} = N_{\text{stars}}/\text{arcsec}^2 \cdot A_{\text{PSF}}$ , with the PSF effective area  $A_{\text{PSF}} = 0.64\text{arcsec}$ .

We illustrate the location of pixels representative of various density brackets on the sky in Fig. 4.

### 3 DECam Plane Survey

To analyze the performance of the LSST Stack with real data, we used the Dark Energy Camera (DECam) imaging, taken as part of the DECam Plane Survey (DECAPS) [9], at the 4-m Cerro Tololo Inter-American Observatory telescope (CTIO)<sup>6</sup>. On Fig. 5 we overlay the locations of all DECAPS fields on top the MAF map of the LSST sky. All DECAPS single-epoch images were

<sup>6</sup>see <http://www.ctio.noao.edu/noao/node/1033>

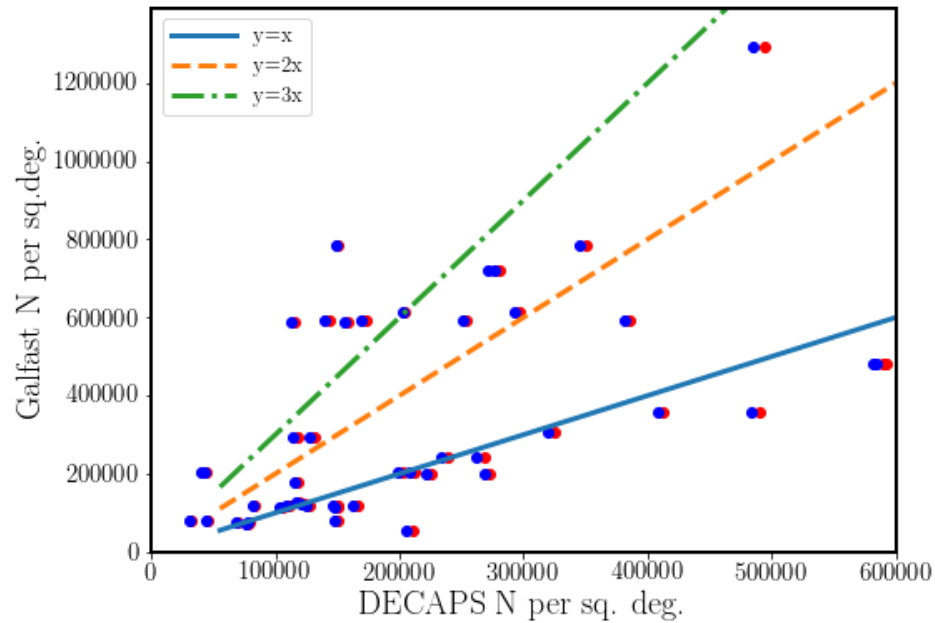


FIGURE 3: Comparison of DECAPS counts in the cleaned catalog (red dots) and raw single-epoch catalog (blue dots), vs. Galfast simulated stellar count in that region of the sky. Overplotted are the line of equivalence  $y=x$ , and its multipicities ( $2x, 3x$ ). It shows that the simulation may be not more accurate than up to a factor of a few, but it is nevertheless useful for defining density regions.

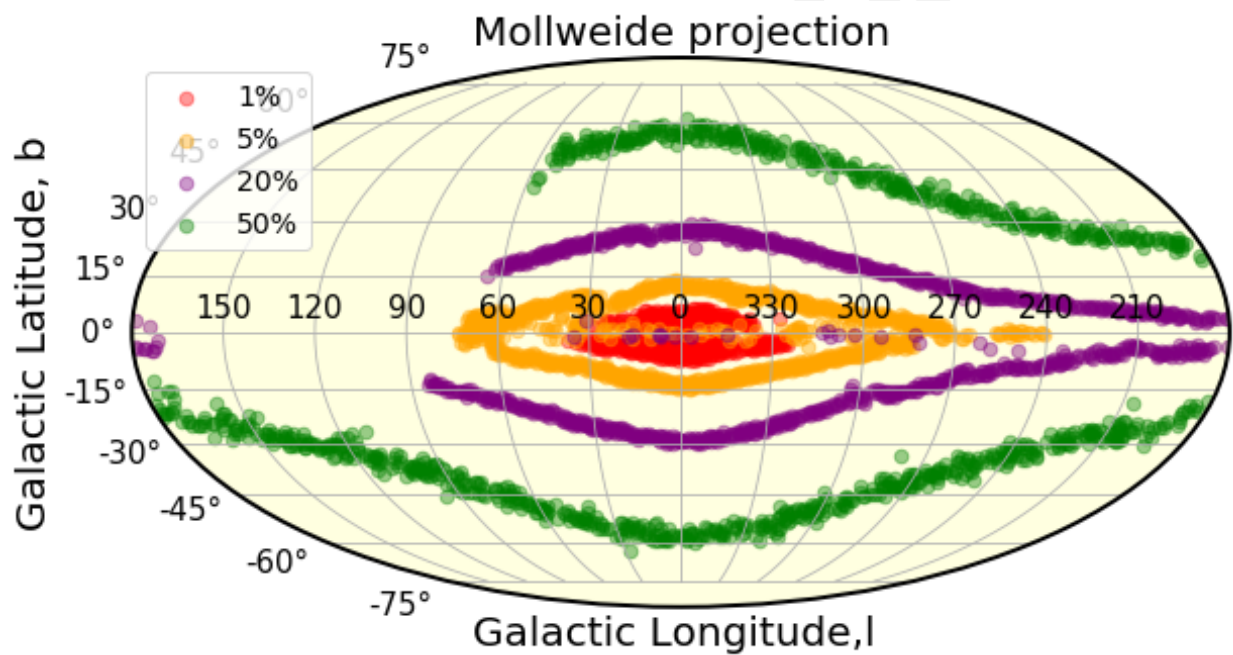


FIGURE 4: Illustration of location of regions representative of different relative simulated stellar densities in cylindrical projection, galactic coordinates. The x% region here means  $x \pm 1\%$ , eg. 5% includes regions between 4-6%. The highest density regions are located close to the galactic bulge, and regions of approximately constant stellar density trace isophotes of the Milky Way. The 20% regions close to the galactic equator correspond to high extinction regions that appear to have less counts due to interstellar dust. The galactic exclusion zone in LSST is closely follows the 5% region outline.

processed with the DECAPS pipeline, resulting in single-epoch catalogs. The details of DECAPS pipeline can be found in Schlaflafy et al. 2017 [9]. The headers of all catalogs were assembled into the image database that contains information about single-visit exposure time, filter, time of observation, position, etc. We used the image database to select DECAPS fields with single-epoch depth similar to that of the single-visit depth of 30 sec LSST exposure. Thus we selected DECAPS fields with exposure between 90 and 125 sec, taken in u, g, r, or VR filter.

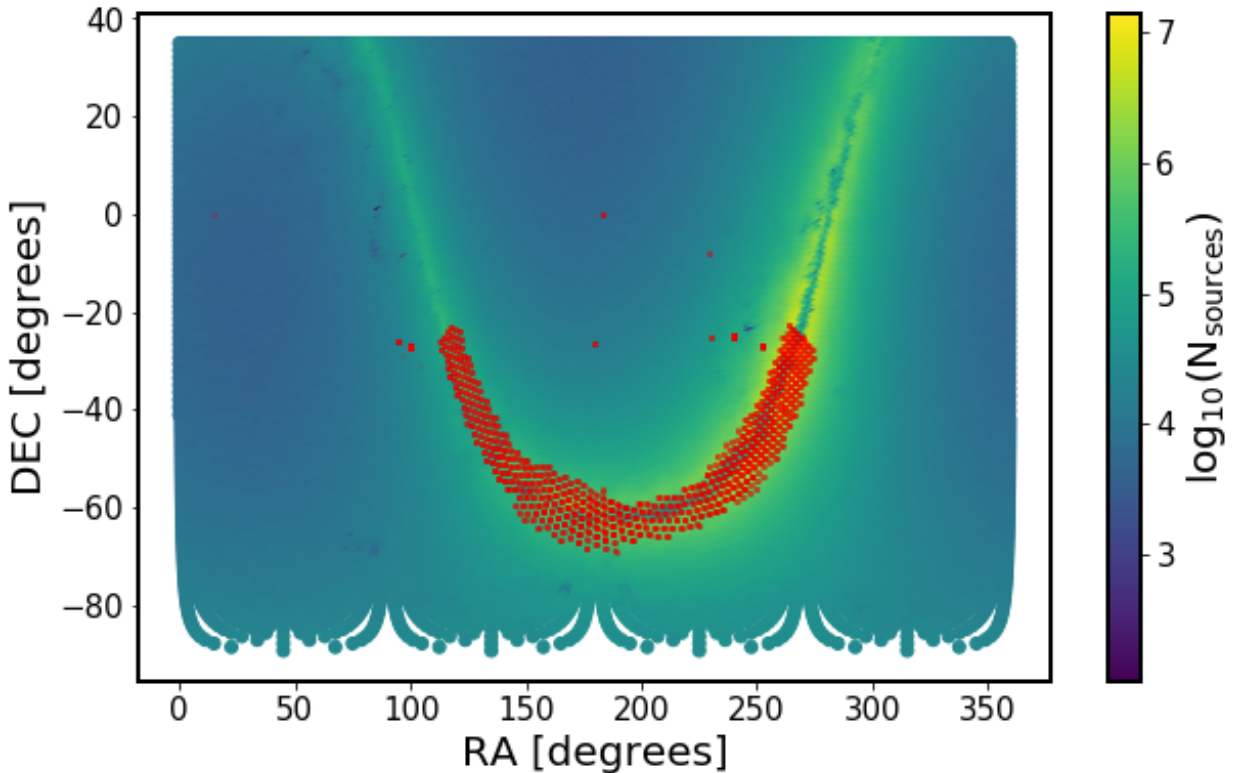


FIGURE 5: All DECAPS fields, overlaid on the map of healpixel stellar densities from MAF simulated sky. We matched the position of the center of each DECAPS field to the nearest healpixel to obtain an estimate of stellar density at each DECAPS field. In this way we selected DECAPS fields representative of various stellar densities (eg. 5%, 10%, 15%, as explained in Sec. 2).

We cross-matched the DECAPS image database with the stellar density information contained in MAF healpixels. Each DECAPS image plane is tiled by a mosaic of 62 CCDs (see Fig. 6). The size of each CCD element of the DECam image plane mosaic is 2046x4094 pixels, with pixel scale of 0.27 arcsec / px, so that a single mosaic element covers an area of 0.047117 square  $\circ$ . A single DECam exposure is also called a visit, and with 62 mosaic elements the full field of view 2.2 $\circ$ wide is several times bigger than the full moon. This makes it comparable to the LSST 3.5 $\circ$ wide field of view. Using the coordinates of the center of each DECAPS field we found the

nearest healpixel within 0.5°.

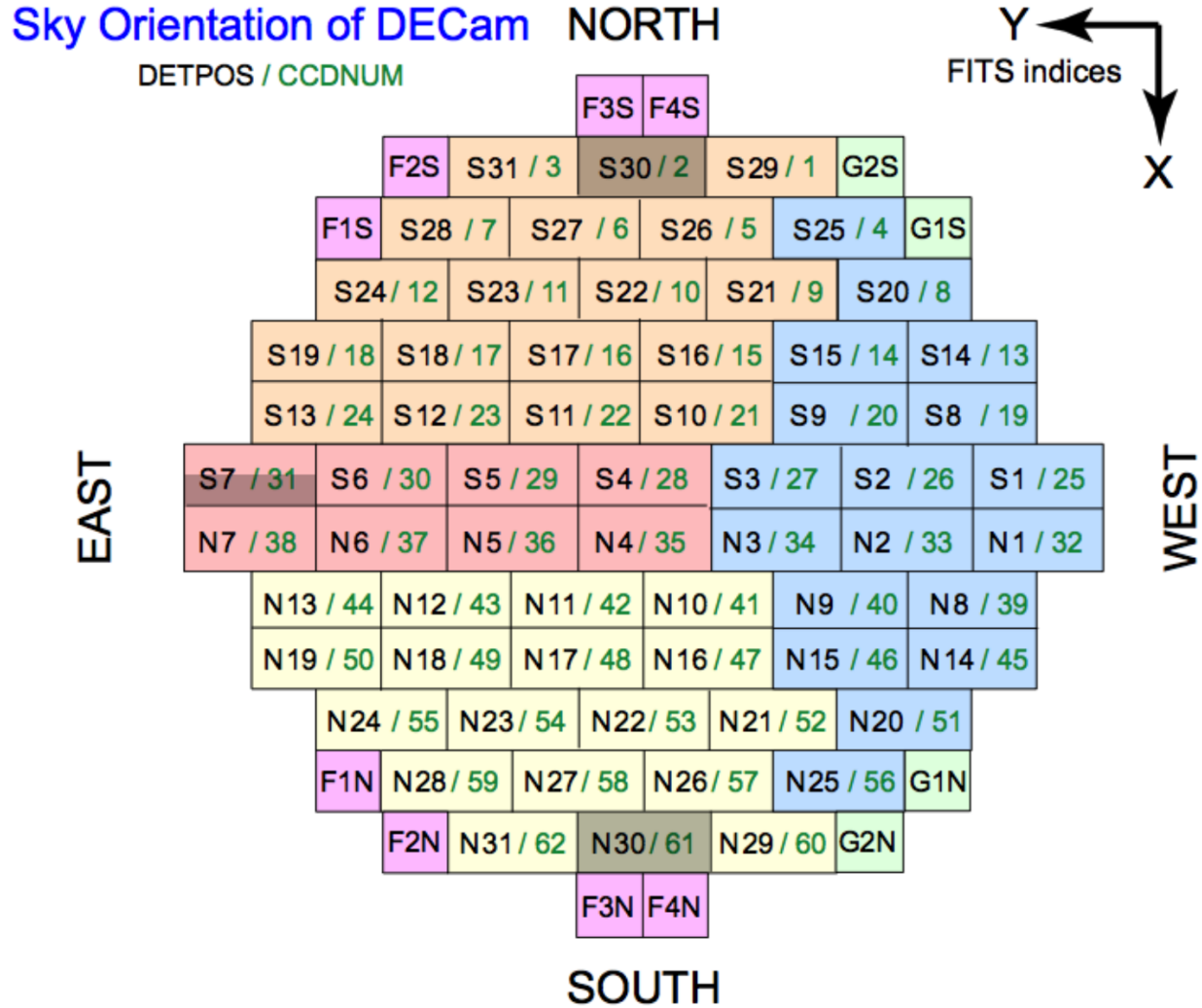


FIGURE 6: An illustration of the DECam CCD mosaic image plane, adapted from Fig.4-3 in NOAO Data Handbook [10]. The color corresponds to the one of the four sets of read-out electronics (orange,pink, blue,yellow), or the guiding (green) and focus (magenta) CCDS. The grey CCDs (S30, S7, N30) did not function properly, and they were excluded from this analysis.

## 4 LSST Processing of DECAPS data

The calibrated DECAPS imaging was processed with the LSST Science Pipelines installed on the LSST-dev machine at the NCSA. We specifically employed processCcd.py and the standard Stack configuration. Transferring the resulting source catalogs and calexp files to a local ma-

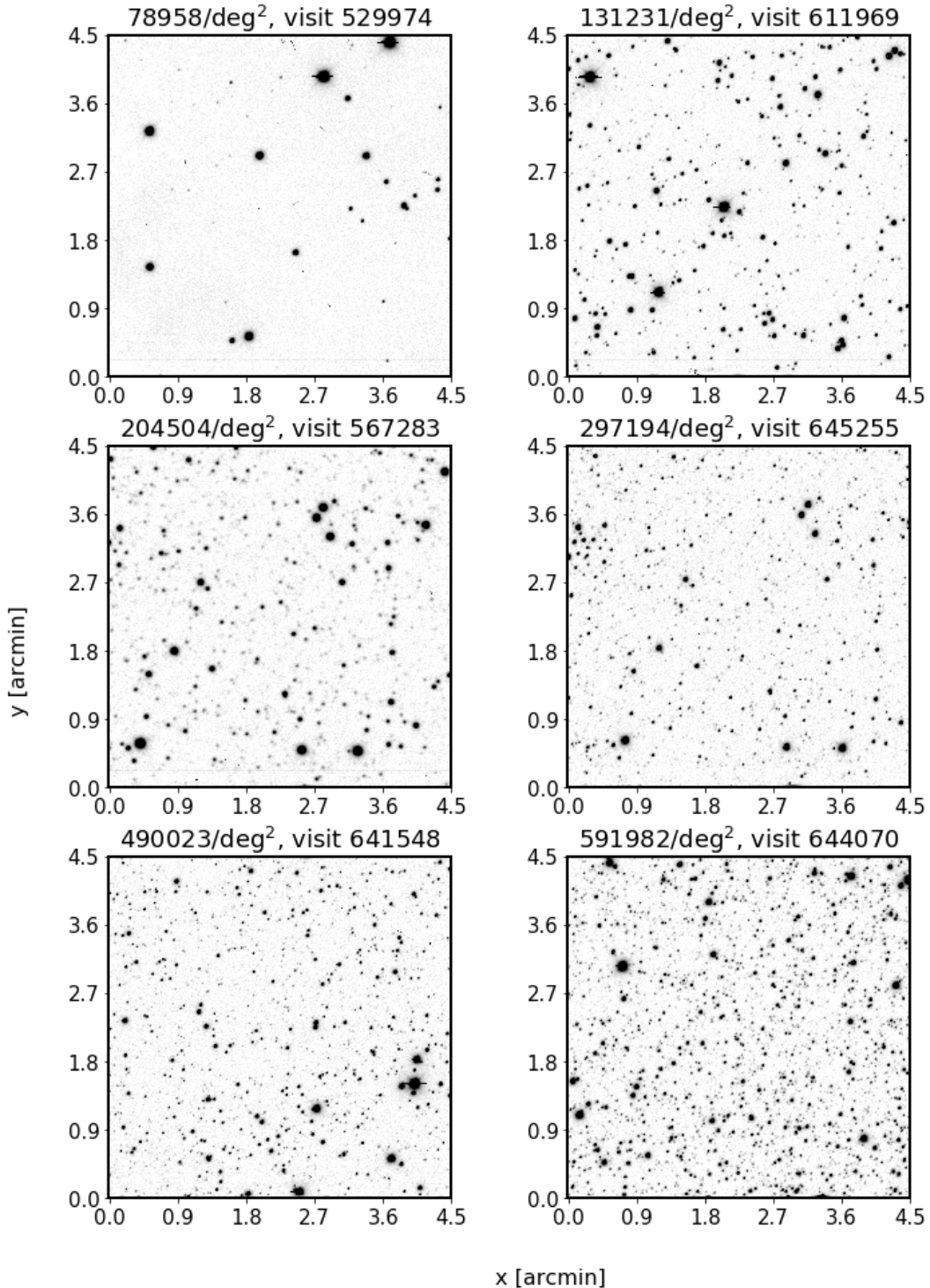


FIGURE 7: Illustration of regions of different stellar count in the cleaned DECAPS single-epoch catalogs. As shown on Fig. 3, the Galfast count (and therefore % level), does not always correspond 1:1 to the actual reported DECAPS stellar count. For this reason we simply ordered all DECAPS fields in terms of source count, and display postage stamp miniatures of CCD regions for visits in regions of increasing stellar density.

TABLE 2: LSST pixel mask bit values.

Bit position	Description	Mask decimal value
0	bad	1
1	saturated	2
2	interpolated	4
3	cosmic ray	8
4	edge	16
5	detected	32
6	detected negative	64
7	suspect	128
8	no data	256

chine we analyzed the output of LSST processing on a laptop using jupyter notebooks and custom python tools. To compare single epoch DECAPS catalogs to LSST source catalogs we used the image mask, deblender flags, and other quality flags. The cleaning process is described in this section.

#### 4.1 Cleaning DECAPS catalog, comparison to LSST pixel mask

To compare LSST and DECAPS catalogs, we cleaned both catalogs using the flag information assigned to each source by the respective image processing pipeline. To verify the validity of DECAPS source flags, we compared them with the LSST pixel-level mask information stored in the FITS Header Data Unit. Pixel-level masks are encoded in 8 bits, each of which can be 'on' or 'off', signifying that a given flag was 'on' or 'off' for a given pixel. The total value of the mask at each pixel is a decimal representation of such eight bits binary number, eg.  $(00100001)_2 = 2^0 + 2^5 = 1 + 32 = (33)_{10}$  means that bit '0' and '5' are 'on' (counting from the right). See Table 2 for details.

For each visit we considered DECAPS single-epoch source catalog, and the LSST calexp image. We combined the calexp image mask value at the nearest pixel to every DECAPS source given its pixel coordinates. The bitwise 'and' of image mask with mask filter  $(11011111)_2 = (2^1 + 2^2 + 2^3 + 2^4 + 2^6 + 2^7)_{10}$  (see Table 2 for details ), flagged the source as 'bad' if either of the flag bits apart from '5' (detected) was 'on'.

Apart from LSST flags, each source also has a DECAPS pipeline flag, the value of which is made up of bits inherited from the NOAO Community Pipeline (see Table 3). We performed a bitwise 'and' of DECAPS flags with the mask filter  $(2^1 + 2^3 + 2^4 + 2^5 + 2^6 + 2^8 + 2^{20} + 2^{22})_{10}$ ,

TABLE 3: DECAPS flags. We excluded sources with flag bits 1,3,4,5,6,8,20,22.

Bit position	Description
1	Bad pixel
3	Saturated
4	Bleed trail
5	Cosmic ray
6	Low weight
8	Long streak
20	Additional bad pixel
21	Nebulosity
22	S7 amplifier B

flagging the source as ‘bad’ if either of these mask bits were ‘on’.

Given the LSST and DECAPS flags, we compared which sources would be excluded based on the DECAPS source-level flags vs LSST pixel-level masks. We found for a random visit 611980 that the overlap between sources excluded by LSST pixel mask information versus DECAPS source flags is 99%. This means that the DECAPS flagging is consistent with the LSST image mask information, and the same sources would be ‘excluded’ based on either DECAPS flags or LSST mask information. For this reason we decided to clean the DECAPS catalog with source level flags, rather than the LSST image mask data.

## 4.2 Cleaning LSST catalog

The LSST source catalog contains for each source a list of 83 flags that could be set ‘on’ or ‘off’. Of these, flags number 60:72 are `base_PixelFlags_flag`, meaning they contain information relevant to the level of source detection, rather than processing (see Table 4 for details).

We clean the LSST source catalog by removing sources that have flags number 62 (edge) or 67 (interpolatedCenter)<sup>7</sup>. Other flags would remove too many sources that have only small ‘defects’, eg. 64 (interpolated) is on for a bright source on the footprint of which there is a cosmic ray, and 65 (bad) is on for any source which has even one bad pixel in the footprint. A comparison of the initial source count to the final source count (after cleaning) is shown on Fig. 10, with detailed count in Table 5.

Given the single-epoch DECAPS source catalogs, and the LSST source catalogs, we followed a

<sup>7</sup>This is similar to the example in Sec.4 of SDSS Image Processing I: The Deblender [3]

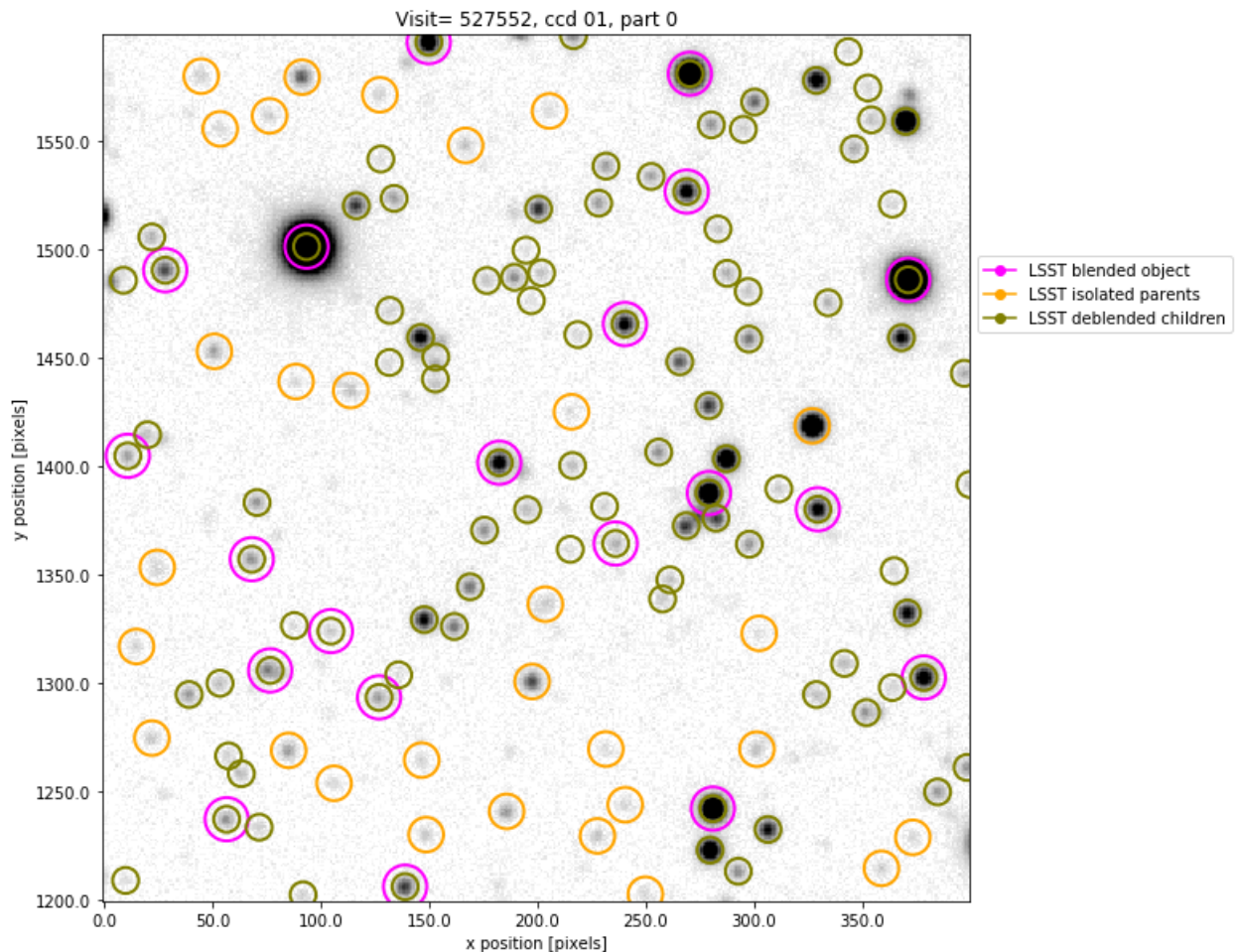


FIGURE 8: We illustrate the sources as reported by the LSST pipeline for a small region of CCD01 of visit 527552. A source may be reported as an isolated source (yellow), or a blend (magenta). If it is a blend, it may become successfully deblended producing deblended children (green). In what follows, we remove blended sources, and only keep isolated parents and deblended children.

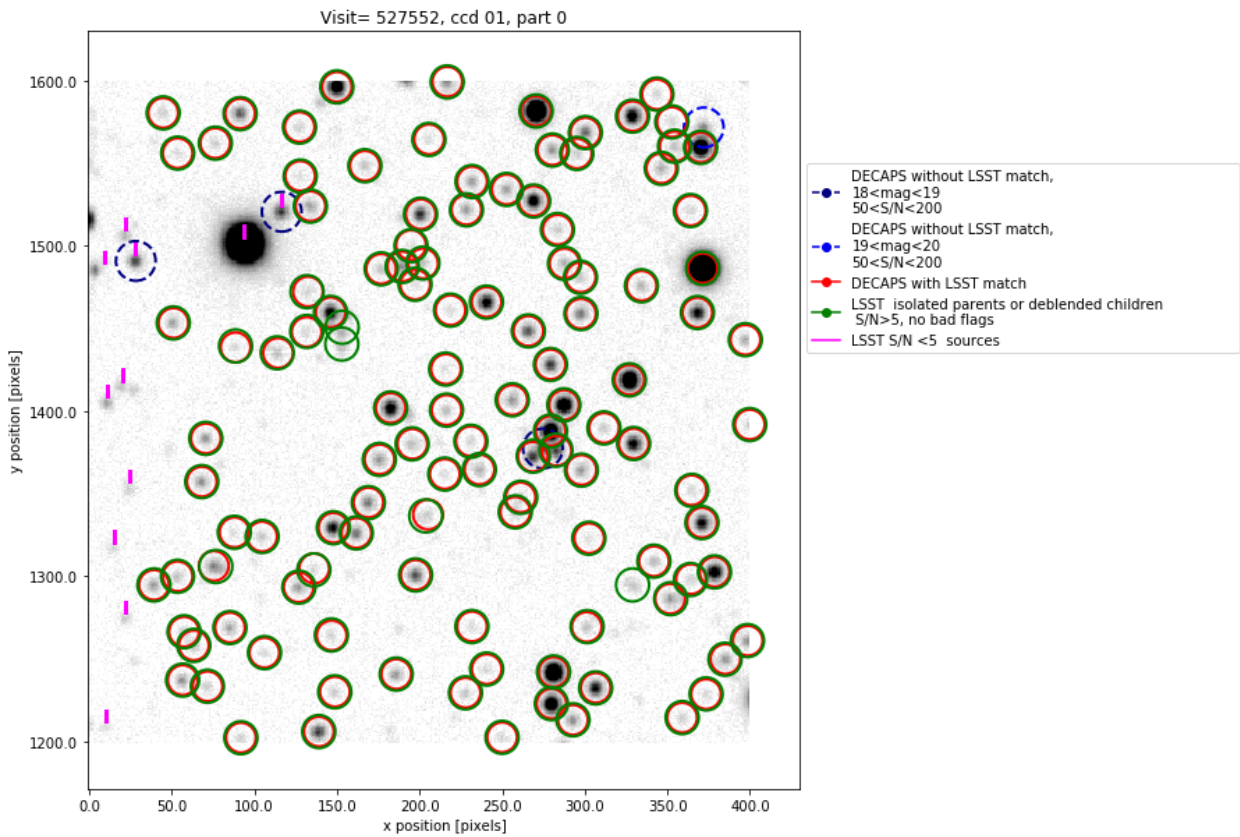


FIGURE 9: The same region as on Fig. 8. Green circles mark the position of retained LSST sources: isolated parents, or deblended children, with  $S/N > 5$ , and no bad flags. Red circles mark the position of DECAPS detections with an LSST match. Vertical magenta dashes are above the LSST sources with  $S/N < 5$ . Blue dashed circles mark location of DECAPS source without an LSST match. Note that e.g. at  $(x,y) = 50, 1490$  an LSST source was detected, but since its  $S/N < 5$  it was not kept in the clean LSST catalog.

TABLE 4: LSST source flags explanation. All flags names start with 'base\_PixelFlags\_flag\_' which was omitted in the flag\_name column below.

number	name	explanation
60	flag	general failure flag, set if anything went wrong
61	offimage	Source center is off image
62	edge	Source is outside usable exposure region (masked EDGE or NO_DATA)
63	interpolated	Interpolated pixel in the Source footprint
64	saturated	Saturated pixel in the Source footprint
65	cr	Cosmic ray in the Source footprint
66	bad	Bad pixel in the Source footprint
67	suspect	Source's footprint includes suspect pixels
68	interpolatedCenter	Interpolated pixel in the Source center
69	saturatedCenter	Saturated pixel in the Source center
70	crCenter	Cosmic ray in the Source center
71	suspectCenter	Source's center is close to suspect pixels
72	flag	General Failure Flag

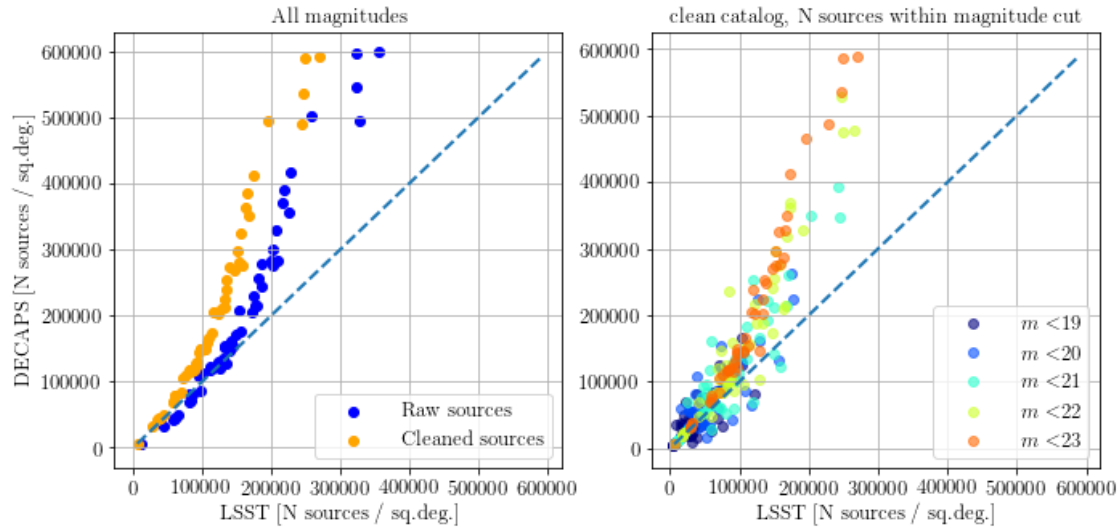


FIGURE 10: A plot of source count comparing LSST to DECAPS source catalogs of the same fields (visits). On the left panel blue dots mark raw source count, i.e. count of the input LSST source catalog or DECAPS single-epoch catalog. The source catalog count was converted to number of sources per square degree, since in some cases not all CCDs were processed. Orange dots mark the count of clean sources (see Fig. ??). As we would expect, between raw and clean catalogs the points on the diagram move vertically from top to bottom, and horizontally from right to left. For exact counts in each stellar field, see LSST counts Table 5 and DECAPS counts Table 6. The right panel shows the effect of excluding faint sources on the clean catalog: selecting only bright sources ( $m < 19$ ), DECAPS and LSST counts for all visits are closer to each other. Only adding faint sources do we reach the situation in the left panel (eg.  $m < 23$ ), where LSST significantly loses faint sources.

TABLE 5: A summary of all LSST-processed DECAPS visits. The column ‘visit’ corresponds to the DECAPS visit number. The following four columns (‘N raw’, ‘N f’, ‘-N r’, ‘=N c’) contain the source counts per visit area ( $\approx 2.74 \text{ deg}^2$ ). ‘N raw’ is the input number of sources per visit , summing over all CCD source catalogs. ‘(N f)’ is the number of sources removed due to bad flags. ‘-N r’ is the total number of removed sources ( due to flags, low S/N, or sources that in the LSST deblending process are neither isolated parents, nor deblended children). ‘=N c’ is the final number of clean sources per visit (‘N raw’ - ‘N r’= ‘N c’). ‘N c/deg<sup>2</sup>’ is ‘=N c’ converted to count per deg<sup>2</sup>. N MAF/deg<sup>2</sup> is the predicted number of sources per deg<sup>2</sup> at that location based on Galfast simulation.  $\rho_{MAF}$  is the MAF density; eg. 21.3 is the top 21.3% stellar density of the simulated sky.

Visit	$N_{\text{raw}}$	$(N_f)$	$-N_r$	$= N_c$	$N_c/\text{deg}^2$	$N_{MAF}/\text{deg}^2$	$\rho_{MAF}$	$N_{loSN}$	$N_{\text{parents}}$	$N_{\text{blend}}$
568172	29809	9148	12434	17375	6241	72072	21.3	12986	153919	7772
527319	120862	13744	39638	81224	29175	79632	19.9	34282	112848	2821
530012	160406	15210	61337	99069	35585	203040	10.6	51669	20425	214
525846	167582	15247	63295	104287	37459	203040	10.6	51949	96932	3172
525900	171337	15037	58219	113118	40631	79632	19.9	46796	70011	973
529989	182933	15910	61808	121125	43508	79632	19.9	49120	114760	5474
529974	228849	16842	67339	161510	58014	76572	20.5	44712	104406	2698
525814	235307	16811	72214	163093	58582	76572	20.5	50998	98063	2812
527096	227256	16100	59686	167570	60191	55908	25.0	36748	85483	1613
644125	242521	16387	72363	170158	60101	72072	21.3	40731	89237	1786
611980	273032	18816	76043	196989	70758	116856	15.6	41383	78662	4251
527247	264383	15283	66539	197844	71065	116676	15.6	38391	138758	5972
567283	280305	16981	68379	211926	76123	612648	4.0	30908	230049	6459
527555	313294	1173	81585	231709	83229	783324	3.0	39458	127709	4957
612757	317270	4014	84877	232393	82084	292788	7.9	42468	128543	5064
527246	319929	18136	86268	233661	83930	114588	15.7	47233	128325	5865
640891	355861	24520	107462	248399	87737	121536	15.1	60163	127665	4569
611970	377917	26716	120640	257277	92413	178992	11.5	80884	133384	5352
645251	348033	18786	89669	258364	91257	128016	14.7	41210	129397	3413
527296	361951	21167	101452	260499	93571	588096	4.2	63149	144777	5063
611969	387056	25752	118639	268417	96415	292788	7.9	74291	162439	7030
526413	368017	22267	98745	269272	96722	78480	20.1	52626	151602	8267
525838	371329	19984	100644	270685	97229	116676	15.6	54839	71782	1611
525837	393879	22350	107414	286465	102898	114588	15.7	56743	74171	1458
611529	398924	22625	105677	293247	105334	116856	15.6	54741	113152	8653
527552	395446	1716	99214	296232	106406	591336	4.2	44093	95415	7272
525920	415231	22439	111423	303808	109127	588096	4.2	59375	133660	5528
527300	436689	24839	120330	316359	113635	594324	4.2	70470	170980	8268
644035	435830	2170	106363	329467	116371	205308	10.5	46535	93985	4830
525904	479294	26679	135534	343760	123478	594324	4.2	77080	112960	6774
527453	495629	28732	139172	356457	128039	242316	9.3	80487	208259	1378
609754	490143	26233	121738	368405	132330	116856	15.6	62319	199832	1515
530032	486203	23112	115217	370986	133257	198432	10.7	51002	176645	1130
526152	520842	28739	143336	377506	135599	55404	25.1	77724	142876	1000
567795	508405	26663	129592	378813	136069	721728	3.4	63447	62120	4248
641497	529827	28546	137626	392201	138530	205308	10.5	59868	184493	1396
640995	571174	2973	155705	415469	146748	242316	9.3	85262	171899	6766
527064	558264	26197	132299	425964	153006	591336	4.2	56098	184352	5900
566793	560376	1088	134186	426190	158458	1292976	1.7	59842	132416	6062
644205	571378	4663	142463	428915	151498	721728	3.4	65955	165636	4585

TABLE 6: A summary of all single-epoch DECAPS source catalogs, with columns as in Table 5. See Fig. 10 comparing the 'N raw' converted to number of sources per square degree, and 'N clean per sq.deg.'

Visit	$N_{raw}$	$(N_f)$	$-N_r$	$= N_c$	$N_c/\text{deg}^2$	$N_{MAF}/\text{deg}^2$	$\rho_{MAF}$
568172	16824	138	150	16674	5989	72072	21.3
527319	92326	2819	3039	89287	32071	79632	19.9
530012	121313	3293	3982	117331	42145	203040	10.6
525846	125245	3135	3457	121788	43746	203040	10.6
525900	127722	2557	2786	124936	44876	79632	19.9
529989	140043	2527	2803	137240	49296	79632	19.9
527096	194837	2126	2290	192547	69162	55908	25.0
525814	200562	4481	4938	195624	70268	76572	20.5
529974	224231	3992	4413	219818	78958	76572	20.5
644125	228088	5570	6182	221906	78380	72072	21.3
527247	237656	4858	5144	232512	83518	116676	15.6
527246	301083	5469	5907	295176	106027	114588	15.7
611980	315722	6779	7397	308325	110750	116856	15.6
527296	330295	7176	7726	322569	115866	588096	4.2
611970	340528	9668	10513	330015	118541	178992	11.5
612757	342629	8541	9473	333156	117674	292788	7.9
645251	343358	5546	6253	337105	119069	128016	14.7
640891	361837	9423	10389	351448	124135	121536	15.1
525838	360793	6057	6515	354278	127256	116676	15.6
611969	376588	10280	11243	365345	131231	292788	7.9
527300	409385	8974	9654	399731	143583	594324	4.2
611529	428299	9981	11167	417132	149833	116856	15.6
527555	421706	3848	4285	417421	149937	783324	3.0
525837	425261	6791	7437	417824	150082	114588	15.7
526413	428035	8417	9137	418898	150467	78480	20.1
525920	449868	6675	7430	442438	158923	588096	4.2
609754	474355	10034	11677	462678	166193	116856	15.6
525904	490306	8413	9118	481188	172842	594324	4.2
567283	575760	5549	6426	569334	204504	612648	4.0
644035	583432	9457	10948	572484	202208	205308	10.5
526152	599164	12579	14023	585141	210182	55404	25.1
641497	611424	10156	11324	600100	211962	205308	10.5
530032	638179	9776	10964	627215	225295	198432	10.7
527453	682113	14654	16569	665544	239062	242316	9.3
527552	714305	6031	6893	707412	254101	591336	4.2
525879	772457	11625	13117	759340	272754	198432	10.7
640995	783011	17946	20850	762161	269204	242316	9.3
567795	791019	9439	11056	779963	280162	721728	3.4
644205	800175	13601	15899	784276	277016	721728	3.4
645255	852539	9620	11135	841404	297194	612648	4.0
641500	935661	14131	16133	919528	324788	305280	7.7
644082	1007998	12826	15633	992365	350515	783324	3.0
526028	1035808	17929	20772	1015036	364600	305280	7.7
527064	1085375	10200	12399	1072976	385412	591336	4.2
644011	1181972	11059	13806	1168166	412611	355896	6.7
566793	1350724	12414	22431	1328293	493863	1292976	1.7

TABLE 7: Summary of possible parentId and nchild combinations for blended sources in the LSST Science Pipeline. An example count in the final column is provided for visit 525814, a top 20% density region, which has the raw source count 235307. For that visit 16811 sources had bad flags, 49901 had  $S/N < 5$ , and in total 163093 were kept in the clean catalog.

parentId	nchild	type	decision	count
0	0	parent: isolated source	keep	104406
0	>0	blended source	remove	26981
!=0	0	deblended child	keep	103920
!=0	>0	failure case	remove	0

uniform set of procedures to clean both datasets, and in turn cross-match positionally. First we made a quality cut removing all sources with signal-to-noise ratio smaller than five:  $S/N < 5$ . The number of sources thus removed depends on a visit number, but does not exceed few % of the catalog. Following that we also removed sources with flags that correspond to bad, edge detections, cosmic rays, or saturation spikes (as outlined in Sec. 4.1 and 4.2). The LSST Processing Pipeline deblends sources in a similar fashion to the SDSS Imaging Pipeline<sup>8</sup>. For the LSST source catalog, we chose to keep only those sources that were either isolated parents ( parentId=0, nchild=0), or deblended children (parentId != 0 , nchild=0) (see Table 7 for details.)

## 5 Metrics

Starting with cleaned LSST and DECAPS source catalogs, we consider a set of metrics to compare the quality of LSST science pipelines to the state-of-the-art DECAPS pipeline.

### 5.1 Completeness

For each visit that corresponds to a given level of crowdedness, we consider the detection completeness of LSST to DECAPS. Assuming that DECAPS is the 'true' catalog of sources, we define completeness by the percentage of DECAPS sources (binned along DECAPS magnitude), that have an LSST match within 0.5''. This is a very liberal requirement considering that for most visits >98% of LSST sources have a match within 0.3''. Second, we require that the sources differ by not more than 0.5 magnitudes. As illustrated on Fig. 14, this only removes the outliers. In fact, given that the majority of the sources (>99%) that are matched within 0.5'', do not differ by more than 0.5 magnitude, this constraint does not change the

<sup>8</sup>SDSS Image Processing I: The Deblender [3], SDSS Image Processing II: The Photo Pipelines [4], [6], and [5]

TABLE 8: Pairs of visits at two different epochs, two per density regime. RA and DEC are in degrees. The separation in arcseconds is between the center of each exposure frame. The last column shows the time difference between the two visits in days.

visit1	ra1	dec1	magzero1	visit2	ra2	dec2	magzero2	d2d "	density
525904	140.5531	-51.24729	29.47	527300	140.5534	-51.24555	29.459	6.3	5
525920	143.2337	-51.44724	29.4465	527296	143.2329	-51.446	29.259	4.8	5
525846	133.5462	-44.27313	29.738	530012	133.5508	-44.27435	29.783	12.6	10
525879	137.6415	-54.08343	29.775	530032	137.642	-54.08628	29.734	10.3	10
525837	131.5622	-48.59523	30.011	527246	131.5601	-48.59695	29.699	7.9	15
525838	132.5935	-50.30486	29.344	527247	132.5894	-50.30705	28.991	12.3	15
525814	126.4261	-43.06979	29.4545	529974	126.4192	-43.07151	29.466	19.2	20
525900	140.6165	-48.15003	29.772	529989	140.6162	-48.15212	29.809	7.6	20

completeness by more than few %. Fig. 11 shows how completeness , and catalog counts, depend on source density.

## 5.2 Photometry

We also considered the photometric accuracy. Since both DECAPS and LSST processing pipelines start from the same instcal calibrated DECam images, they ought arrive at similar measurement of flux, and in turn, instrumental magnitudes. An offset and a spread in magnitude difference is due to details of each image processing pipeline.

We compare the photometric repeatability within each pipeline, as well as the existence of offset and spread between two different pipeines. We test pipeline repeatability by investigating two visits at the same locations, taken in same filters, with equal exposure times. Assuming that the majority of objects are non-variable in nature, we find the statistical epoch-to-epoch variance.

For twelve fields at different stellar densities we found visits at exactly the same location, filter and exposure time, but different observation time (see Table 8). This allowed to compare the spread in photometry epoch-to-epoch within DECAPS, and LSST. We illustrate that plotting the magnitude differences on Figs. 17 and 18, and the summary of the spread of photometric difference as a function of magnitude on Figs. 19 and 20.

We summarize the information about the photometric repeatability (epoch-to-epoch within a given pipeline), and offset (pipeline-to-pipeline of the same epoch), by combining information from Figs. 19, 20, 16. In particular, we characterize the photometric accuracy by a system-

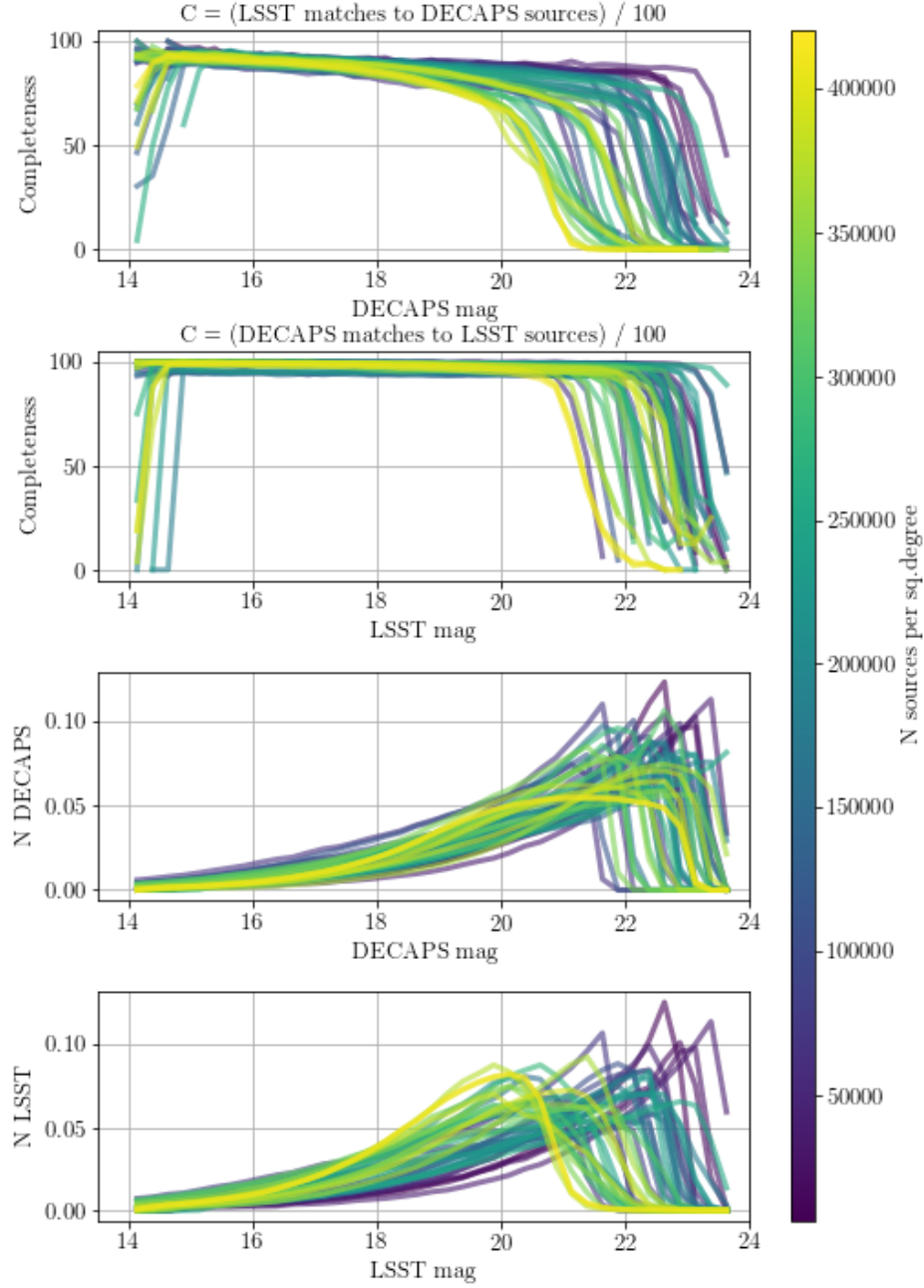


FIGURE 11: Different colors correspond to different level of stellar crowdedness, expressed in terms of number of sources per square degree (the mean between LSST and DECAPS cleaned catalogs). Top two panels show source-to-source completeness. The first of the two top panels is completeness of LSST to DECAPS, i.e. for each DECAPS source we look for an LSST counterpart. The second panel is completeness of DECAPS to LSST , i.e. for each LSST source we find a DECAPS counterpart. The LSST-DECAPS completeness falls off quicker than DECAPS-LSST, since DECAPS catalog has more sources at fainter magnitudes (see Fig. 10). The bottom two panels show the normalized number of counts in the input catalogs. We characterize completeness by two numbers per visit: the mean completeness between 18-20 mag  $\langle C_{18-20} \rangle$ , and the magnitude at which completeness falls to a 50% level,  $m_{50}$ , plotted on Fig. 12.

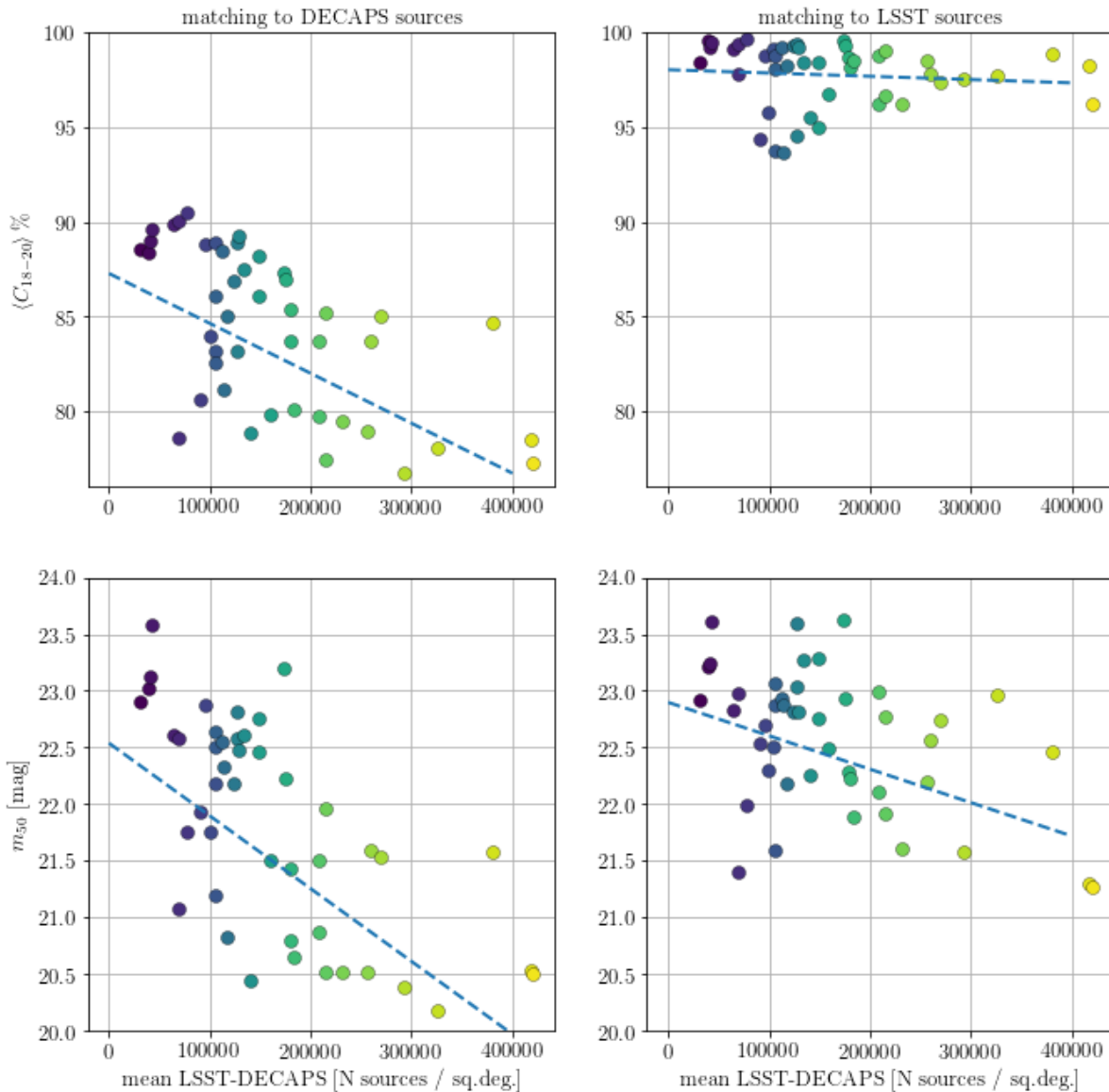


FIGURE 12: Magnitude at which completeness falls to 50% (top two panels), and the mean completeness between 18 and 20 magnitudes (bottom two panels). The panels on the left hand side correspond to the uppermost panel in Fig. 11, while the right hand side panels correspond to the second panel in Fig. 11. The color of all points corresponds to the stellar density, as in Fig. 11. In each panel we overplot the linear best-fit to indicate the expected overall trend of decreasing  $\langle C_{18-20} \rangle$  and  $m_{50}$  with source density.

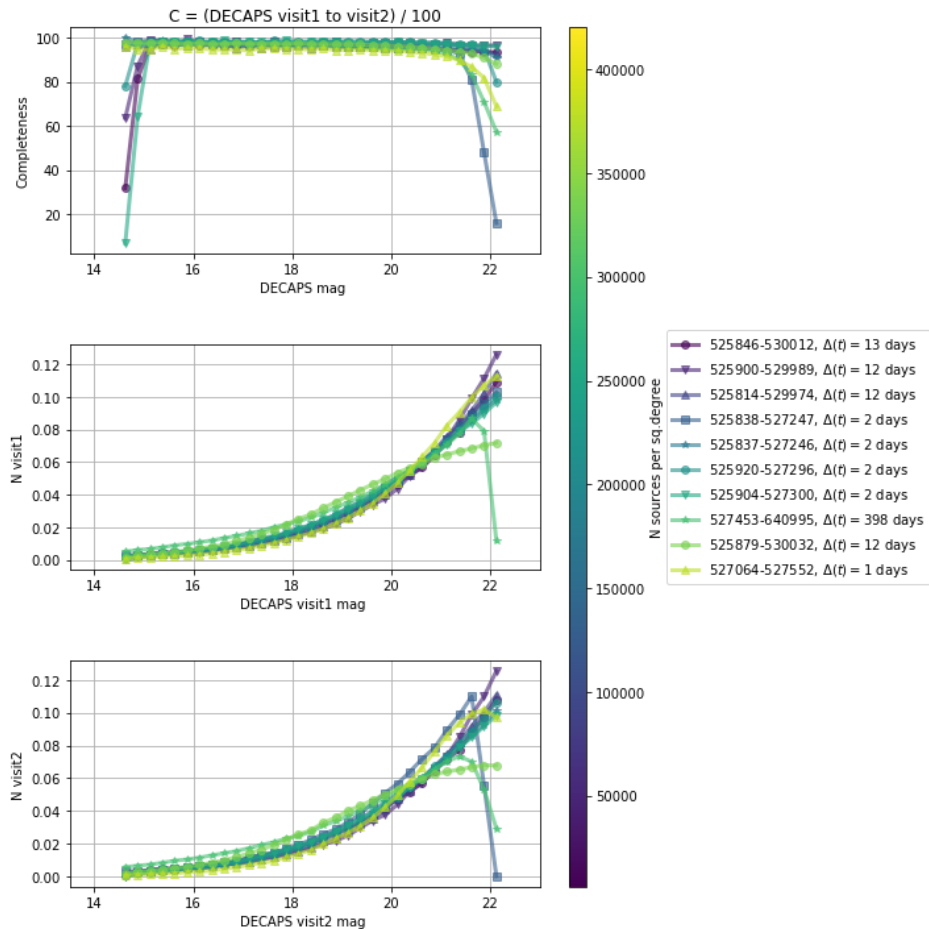


FIGURE 13: The same quantities as on Fig. 11, but corresponding to two different visits at the same location, to test the repeatability of DECAPS detections. The two visits (visit1, visit2) were chosen in the same filter and at the same location, and as in tests for completeness, we match source-by-source and consider the number of sources per magnitude bin in visit1 that do have a matching source in visit2.

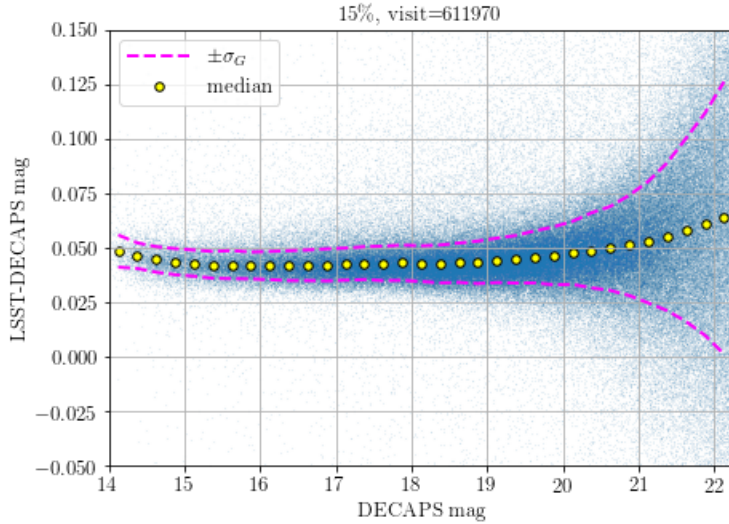


FIGURE 14: Difference in magnitudes between the DECAPS and LSST magnitudes for sources matched within 0.5 "for a region in top 15% density (611970). The magenta dashed line traces the  $\pm\sigma_G(\Delta m)$  level, and yellow circles the median.  $\sigma_G = 0.7413 * (q75 - q25)$ , where  $q75$  and  $q25$  are 75th and 25th percentiles, is an interquartile-based measure of standard deviation, that is insensitive to the outliers. For this stellar density, the offset between LSST and DECAPS is on the level of 0.05 mag. The same quantities ( $\sigma_G$ , median( $\Delta m$ )) plotted for fields of various stellar densities can be shown on Fig. 16. The histograms of  $\Delta mag$  per magnitude bin are shown on Fig. 15.

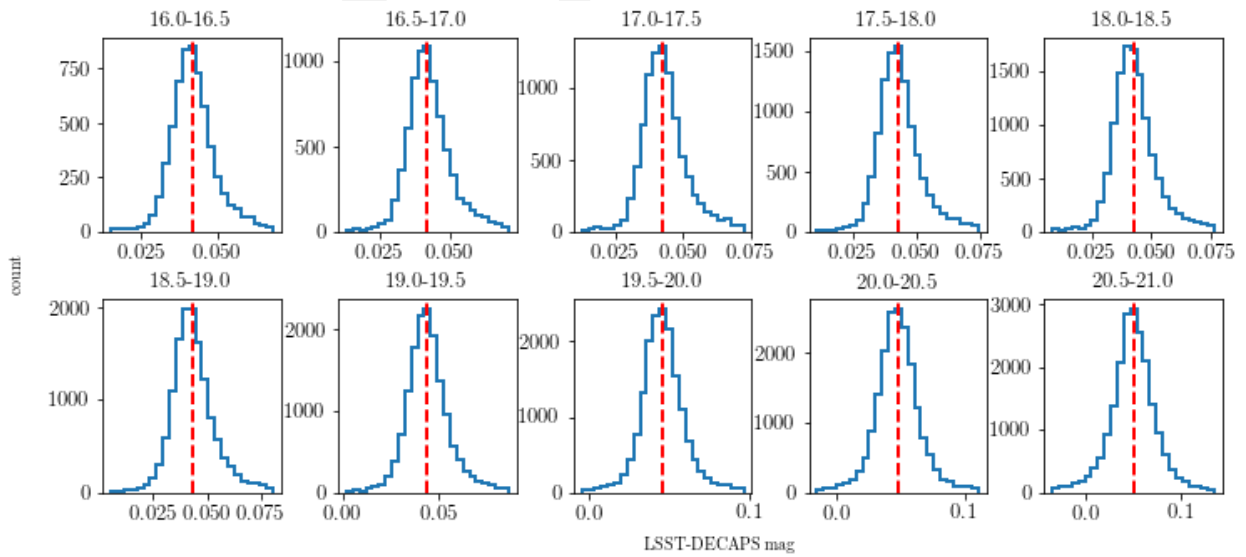


FIGURE 15: Cross-section of Fig. 14, showing the histogram of  $\Delta mag$  per DECAPS magnitude bin. The vertical red line corresponds to the median value of  $\Delta mag$  in that bin, and each histogram is limited between  $\pm 4 \sigma_G$ .

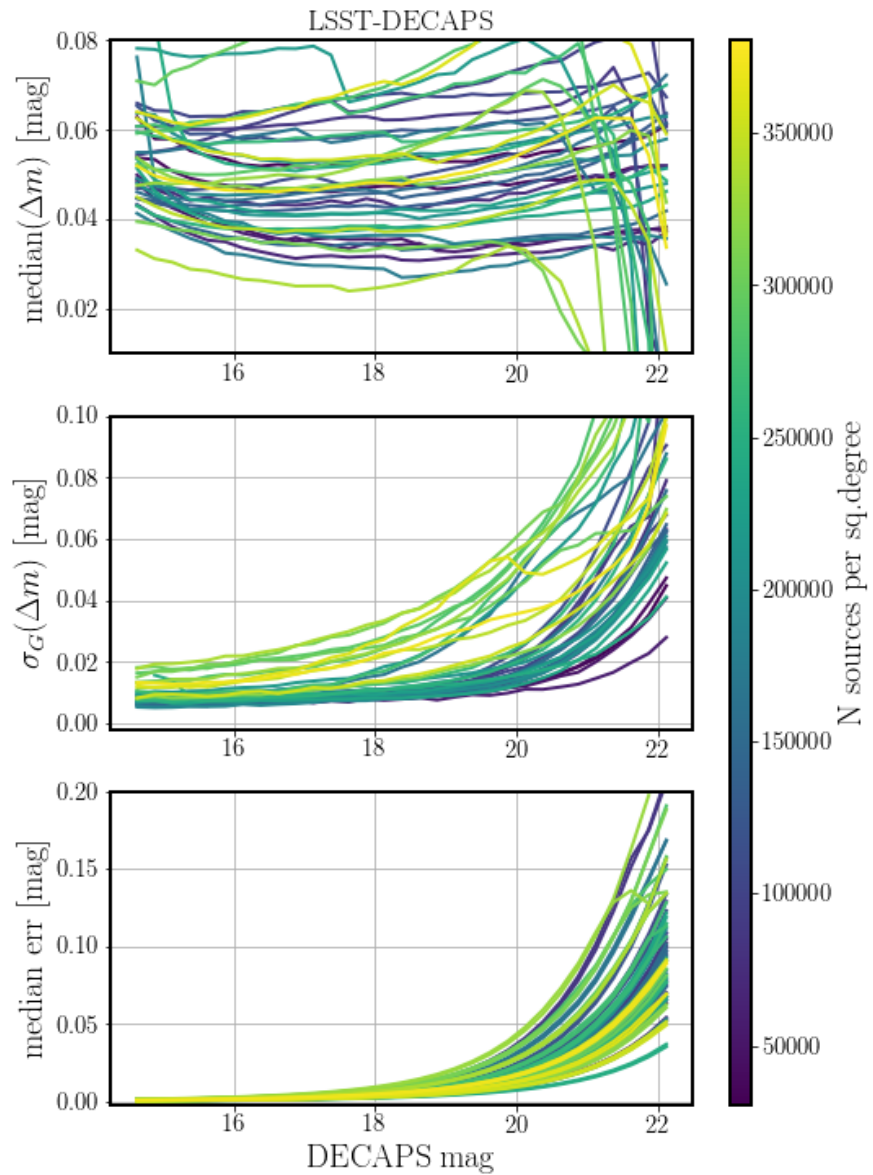


FIGURE 16: The measurement of photometric offset between DECAPS and LSST pipelines. For each visit we cross-matched source catalogs corresponding to LSST and DECAPS processing;  $\Delta m$  is the difference in magnitude reported between DECAPS and LSST for the same source. For each visit we bin sources according to their DECAPS magnitude. On three panels we plot the binned statistics : median  $\Delta m$ ,  $\sigma_G$  - the interquartile-based measure of the spread of the distribution, and median photometric uncertainty.

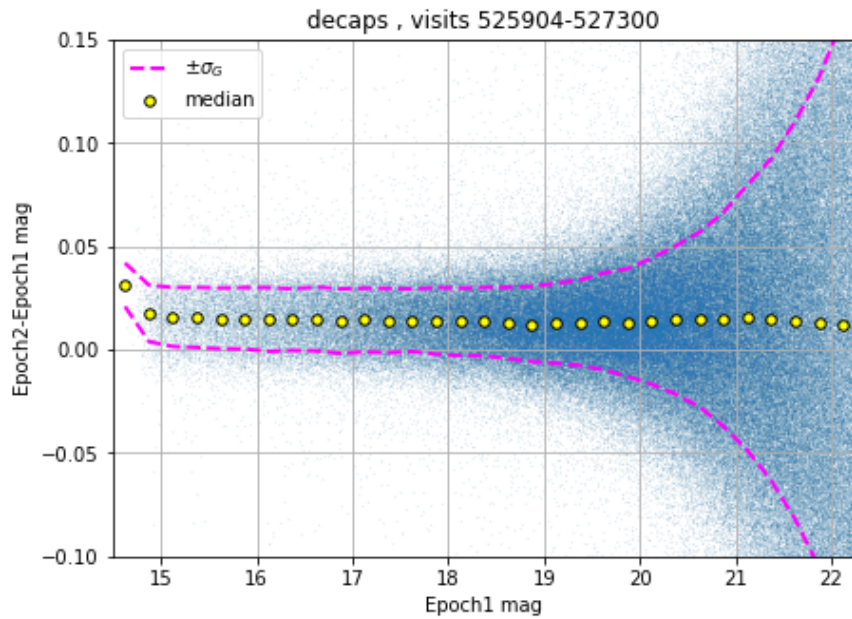


FIGURE 17: Similarly to Fig. 14, scatter plot of the magnitude difference between the two visits (525904, 527300) to the same sky region, separated by 2.95 days, processed by DECAPS. The magnitude difference is shown for all sources cross-matched between the two epochs, with a match within 0.5"- there is no selection on magnitude difference, but 0.5 mag (used for completeness) is well beyond the bounds of the plot, and would only cut the outliers to which neither median nor  $\sigma_G$  are not sensitive. We overplot the  $\pm\sigma_G$  envelope, and the median of each of 0.25 mag bins.

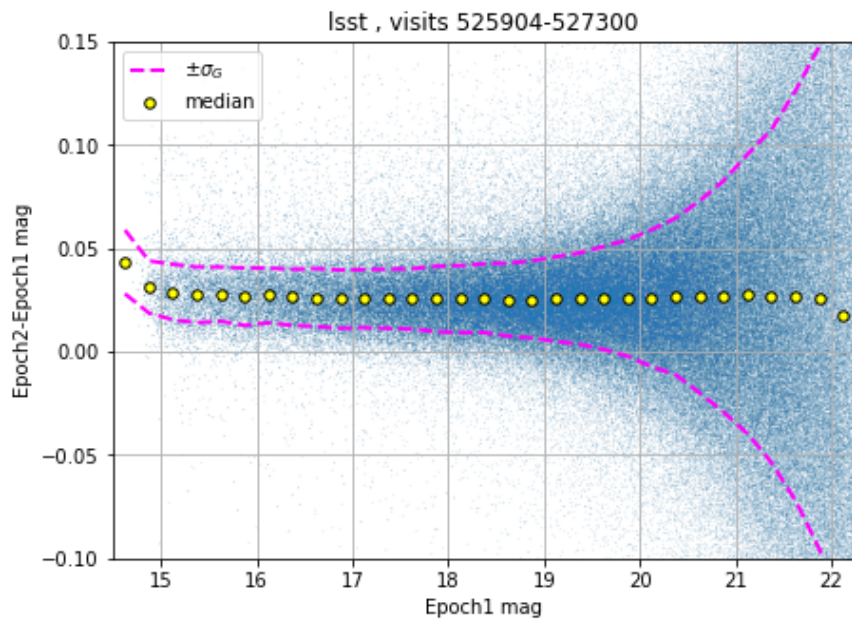


FIGURE 18: The same as Fig. 17, but for LSST processing of two visits to the same region, at two different epochs.

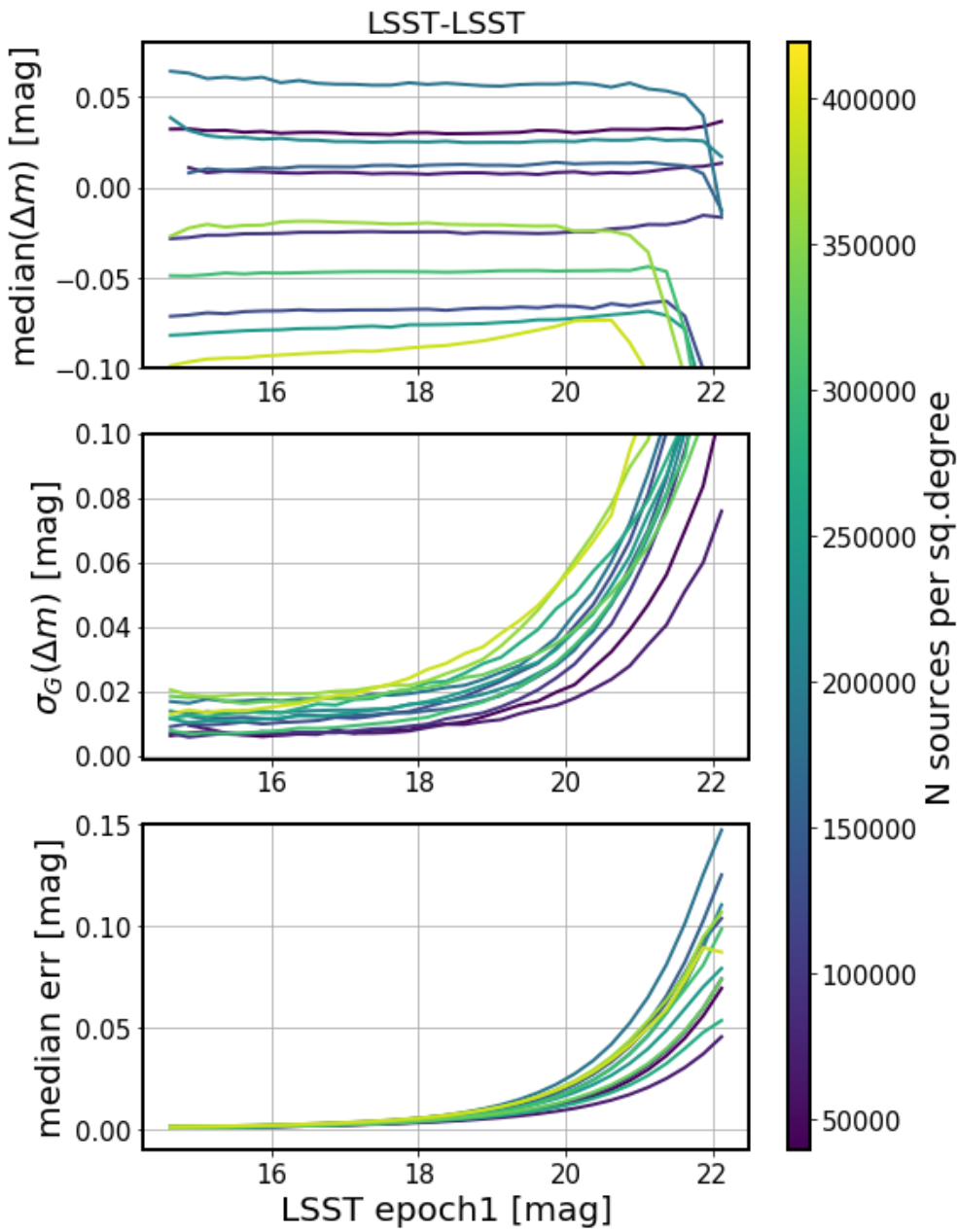


FIGURE 19: The internal repeatability test of the LSST pipeline. We cross-match the source catalogs for each visit. These two brightness measurements for the same source are akin to a two-epoch light curve. Since inherently variable sources constitute a small fraction of all stellar objects, and the majority of stars are not variable, the difference in the measured magnitudes would correspond to the empirical measure of noise. All sources cross-matched within  $0.5''$  are binned according to their brightness. On the panels we plot, from top to bottom: median photometric offset, the robust interquartile-based measure of standard deviation  $\sigma_G$ , and the median reported measurement uncertainty.

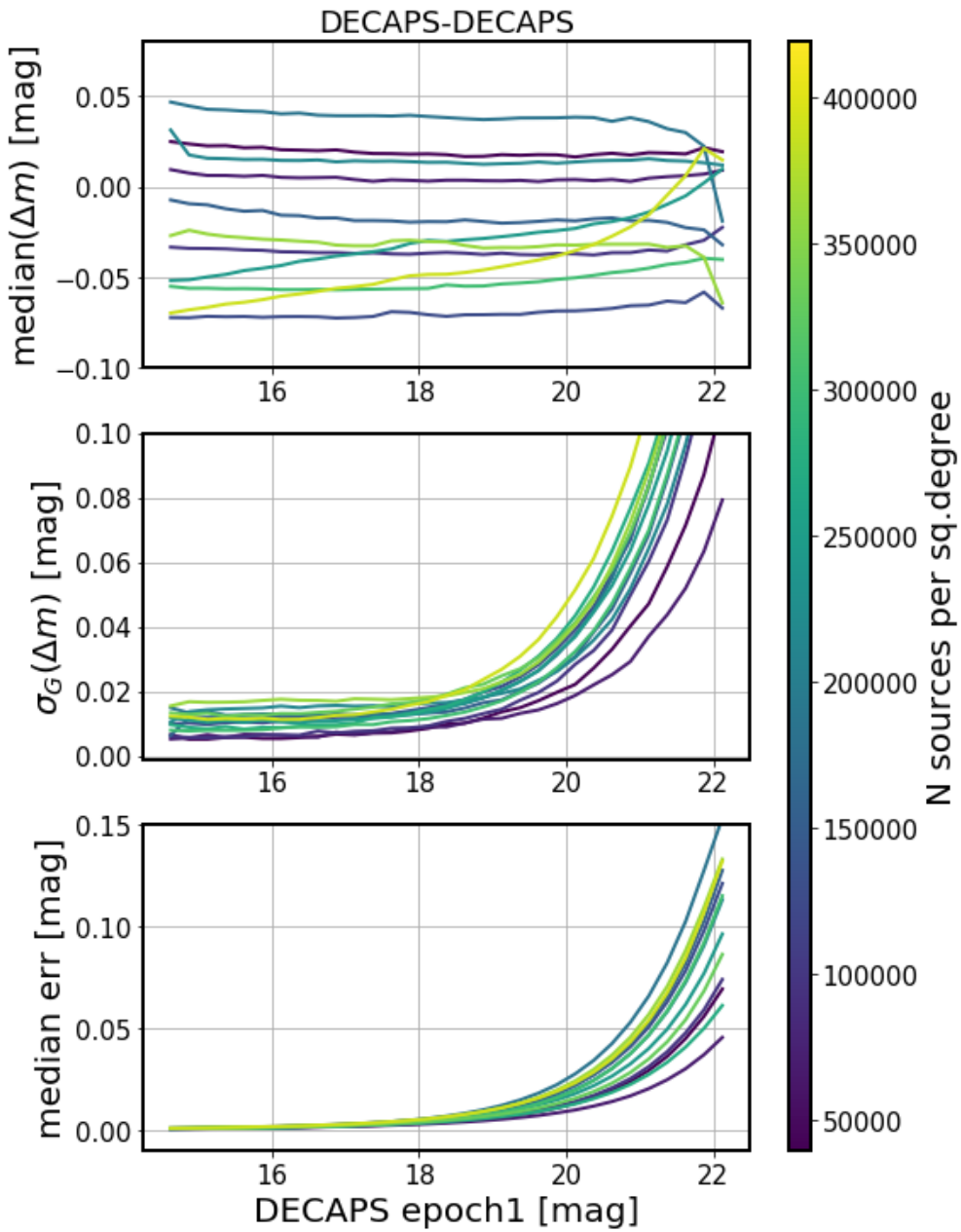


FIGURE 20: The internal repeatability test of DECAPS pipeline - for description, see Fig. 19.

atic offset between the empirical measure of noise and the pipeline-reported photometric uncertainty.

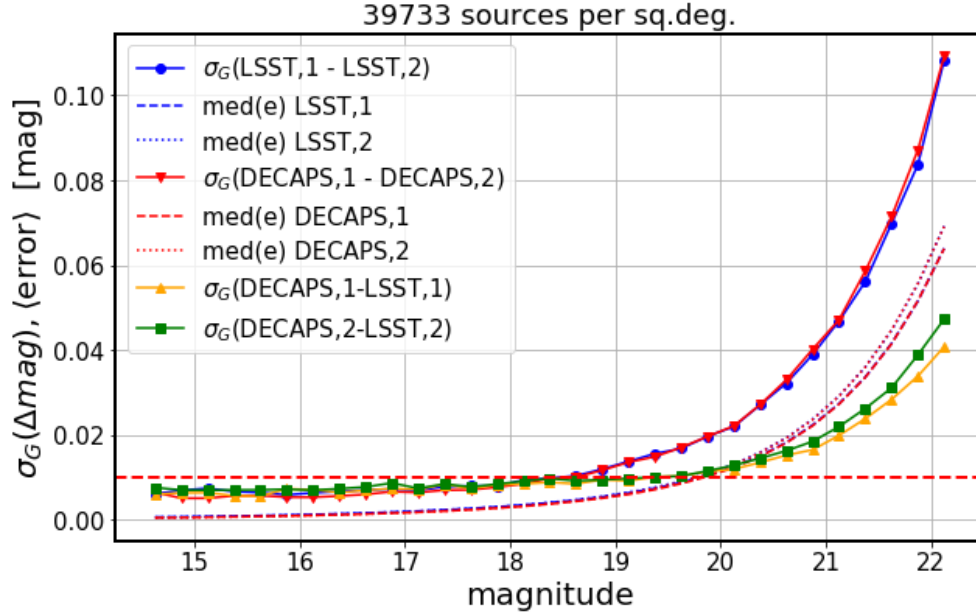


FIGURE 21: Comparison of spread of scatter between two pipelines vs. the empirical measurement of noise from repeatability for a pair of visits at the same location : 525846 and 530012, here called epoch1 and epoch2. All solid lines are  $\sigma_G(a, b)$  - the interquartile-based measure of spread of magnitude difference between measurements  $a$  and  $b$  of the same source. From the top,  $\sigma_G(LSST, 1 - LSST, 2)$ , and  $\sigma_G(DECAPS, 1 - DECAPS, 2)$ , correspond to the empirical measure of noise. The blue line  $\sigma_G(LSST, 1 - LSST, 2)$  is the same quantity as that plotted on the middle panel of Fig. 19, while the red line  $\sigma_G(DECAPS, 1 - DECAPS, 2)$  is the same as that of Fig. 20. Then the dotted and dashed lines in the middle show the median error for epoch 1 or epoch 2, as reported by LSST or DECAPS pipelines. They represent the expected uncertainty in repeated measurement. Since they are identical, the red and blue dotted or dashed lines overlap. Finally, the green and orange solid curves correspond to the scatter between the two pipelines , calculated either for epoch1 ( $\sigma_G(DECAPS, 1 - LSST, 1)$ ), or epoch2 ( $\sigma_G(DECAPS, 2 - LSST, 2)$ ). Fig. 22 shows the second step in the analysis.

## 6 Astrometry

Astrometry corresponds to the measurement of the position of sources in the absolute World Coordinate System (WCS). Accurate and precise astrometry enables for instance catalog cross-matching, and over long-term - measurement of proper motion of stellar sources.

We consider two properties of successful astrometry. First, the internal consistency of pipeline

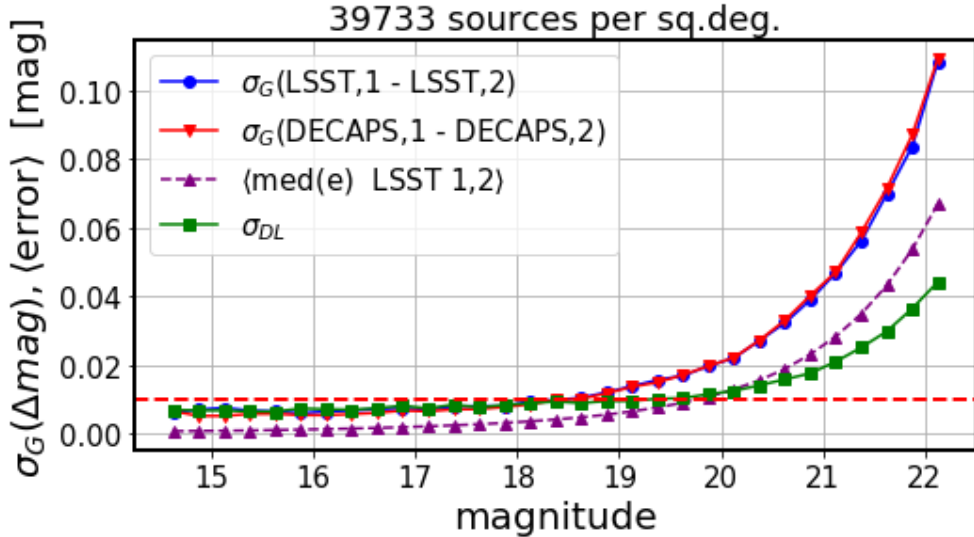


FIGURE 22: Second step in the analysis of photometric spread, following Fig. 21. The blue and red lines of repeatability are unchanged. Since LSST and DECAPS errors are almost identical, we choose to represent the minimum statistical offset by the mean LSST error between the two visits , added in quadrature . If  $e_{1L}$  and  $e_{2L}$  are LSST-reported error measurements for a given source for the two epochs, the quadrature-mean is  $e_{12} = \sqrt{e_{1L}^2 + e_{2L}^2}/\sqrt{2}$ , and the purple dashed line is the median of  $e_{12}$  per magnitude bin. We also add in quadrature the spread between the two pipelines, represented on Fig. 21 by orange  $\sigma_{DL,1}$  for epoch1, and green  $\sigma_{DL,2}$  for epoch2 :  $\sigma_{DL} = \sqrt{\sigma_{DL,1}^2 + \sigma_{DL,2}^2}/\sqrt{2}$ . Note that since the top blue (or red) lines  $\sigma_G(LSST, 1 - LSST, 2)$ ,  $\sigma_G(DECAPS, 1 - DECAPS, 2)$  ( $\sigma_{DD}$ ,  $\sigma_{LL}$  for short) consists of noise  $\sigma_E$  and the systematic offset  $\sigma_S$  :  $\sigma_{LL}^2 = \sigma_S^2 + \sigma_E^2$ . Thus we calculate the systematic offset for LSST as  $\sigma_S = \sqrt{\sigma_{LL}^2 - \sigma_E^2}$ , which is the difference between blue solid and purple dashed lines.

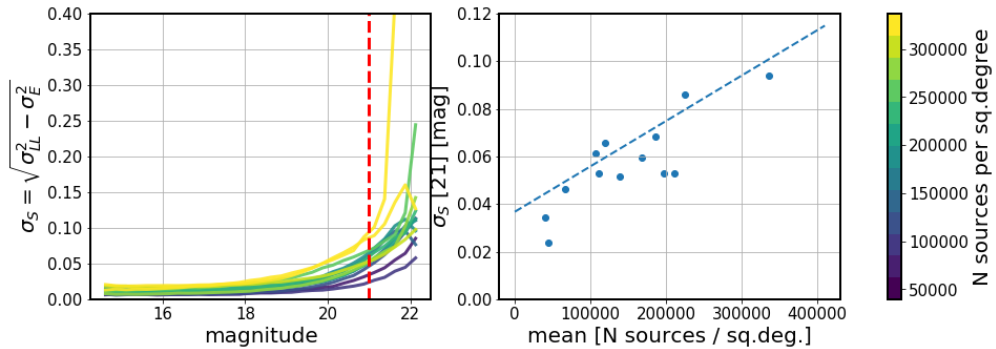


FIGURE 23: The left panel shows the measure of systematic offset between mean photometric error, and the photometric repeatability for the LSST pipeline as a function of magnitude (see Figs. 21, 22. Colors correspond to mean stellar density. Right panel shows  $\sigma_S$  at 21st magnitude as a function of stellar density.

TABLE 9: The difference in RA,DEC for various visits, between LSST processing of fields at the same location, but observed at different times ( see Table 8 for summary). The median and spread of astrometric offset are in miliarcseconds. The final column shows the mean source count between the two visits per square degree.

visit1	visit2	med( $\Delta\alpha$ )	med( $\Delta\delta$ )	$\sigma_G(\Delta\alpha)$	$\sigma_G(\Delta\delta)$	$\langle N \rangle$
525846	530012	1.83	0.18	9.43	8.85	39733
525900	529989	-3.12	0.36	10.87	11.58	44577
525814	529974	-0.29	1.15	10.65	10.46	66455
525838	527247	2.52	-2.23	9.96	12.21	94766
525837	527246	1.58	-1.24	9.07	11.51	110734
525920	527296	0.88	-3.2	10.36	9.85	119371
525904	527300	0.43	-1.55	8.29	10.0	138384
641497	644035	2.26	-1.42	19.8	22.68	167267
567283	645255	-5.58	1.05	33.77	19.75	185894
644082	527555	-4.16	-5.05	29.92	26.1	186731
527453	640995	-0.33	1.7	12.95	12.25	195763
525879	530032	0.8	-0.46	10.56	13.41	197058
527064	527552	-0.13	-2.19	16.93	15.74	224731
526028	641500	-1.2	0.42	11.52	11.12	281929
641548	644011	1.2	-2.43	26.08	30.7	336729
644144	566793	1.05	-0.25	27.86	19.69	339183
644074	644070	-2.56	0.3	26.14	27.69	419000

by measuring the repeatability of astrometric measurement between different epochs. Second - accuracy, in particular, any possible biases between two different pipelines.

DECAPS used 2MASS and GAIA for the astrometric calibration [9], while LSST Pipelines use the GAIA-TGAS astrometric solution.

We correct the offset in  $\alpha$  :  $\Delta\alpha_{corr} = \delta\alpha \cos(\delta)$

To test repeatability we use pairs of observations at the same location. Fig. 24 shows an example of the LSST-LSST comparison, with Fig. 25 showing the magnitude dependence. Fig. 26 shows the offset in  $RA, DEC$ , for DECAPS-DECAPS comparison.

To test possible offset between LSST and DECAPS astrometric solutions, on Fig. 29 we find the offset in measured  $RA, DEC$  for sources cross-matched in catalogs from the two pipelines.

## 7 Future work

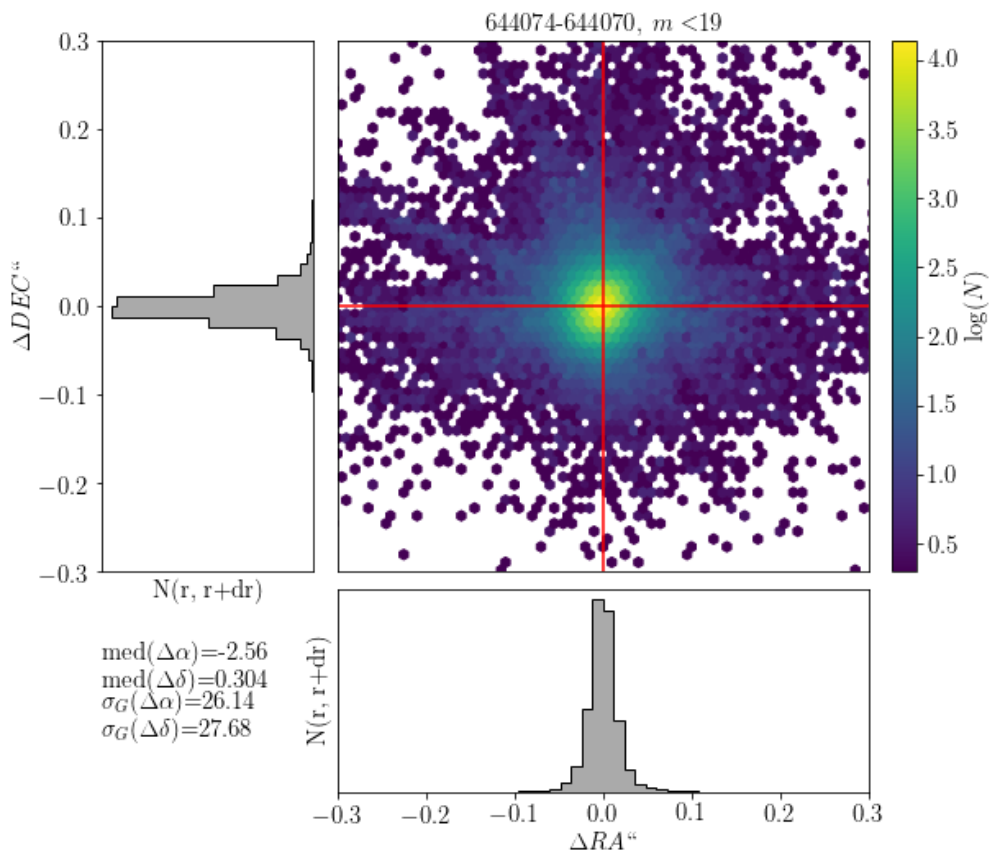


FIGURE 24: The difference of LSST processing for RA,DEC for visits 644074,644070: a pair of visits at the same location, separated by less than a day. The mean number of sources is 419000 sources per sq.deg., which corresponds to top 1% of the sky. We select sources brighter than 19 magnitude. For all other pairs the offsets are all centered on zero with similar spread - see Table 9

LSST processing, visits 644074-644070 mean 419000 sources per sq.deg.

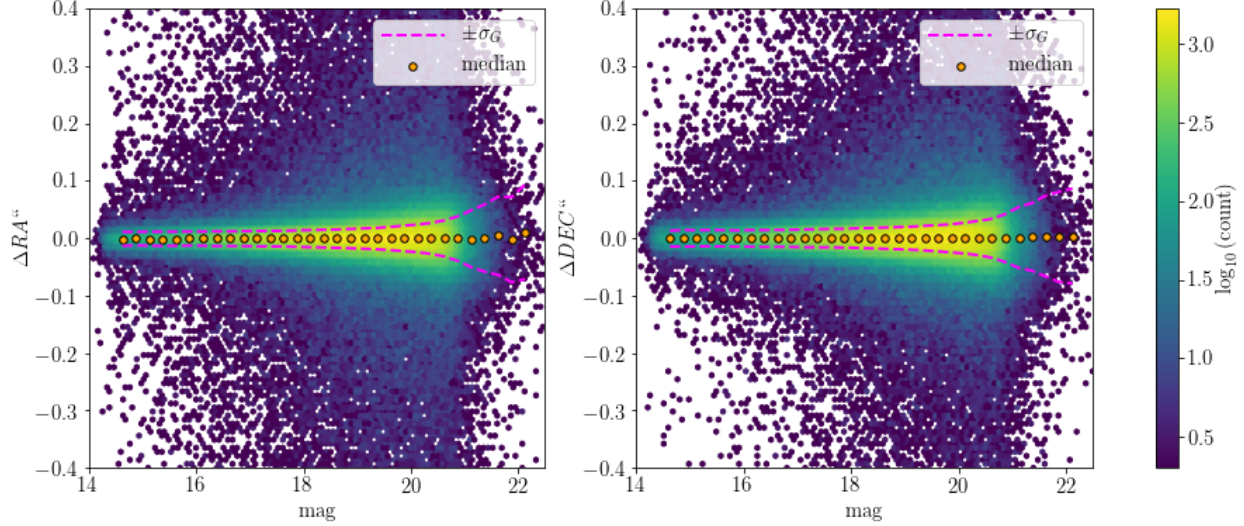


FIGURE 25: The difference in RA,DEC for the same visits as on Fig. 24, shown as a function of magnitude.

TABLE 10: The difference in RA,DEC for various visits, between DECAPS processing of fields at the same location, but observed at different times ( see Table 8 for summary). All measured quantities are in milliarcseconds. See Table 9 for the equivalent visits processed by LSST.

visit1	visit2	med( $\Delta\alpha$ )	med( $\Delta\delta$ )	$\sigma_G(\Delta\alpha)$	$\sigma_G(\Delta\delta)$	$\langle N \rangle$
525846	530012	5.92	-1.18	14.69	14.49	39733
525900	529989	-5.34	-4.18	21.18	20.76	44577
525814	529974	6.55	0.19	20.58	17.76	66455
525838	527247	-6.5	-0.72	17.62	16.45	94766
525837	527246	-3.55	-2.86	18.5	17.57	110734
525920	527296	-4.97	-3.26	19.72	16.88	119371
525904	527300	-5.05	-4.13	14.4	16.26	138384
641497	644035	8.91	12.57	34.18	31.02	167267
567283	645255	-53.12	-49.23	39.71	24.55	185894
644082	527555	139.33	-15.63	40.71	36.27	186731
527453	640995	-126.51	28.81	24.75	18.27	195763
525879	530032	-0.43	-5.17	22.88	23.66	197058
527064	527552	5.11	-3.74	20.95	25.13	224731
526028	641500	-134.26	28.5	26.81	19.56	281929
641548	644011	-1.69	-5.63	32.3	36.95	336729
644144	566793	94.95	68.82	32.42	23.74	339183
644074	644070	-4.92	1.61	25.15	28.14	419000

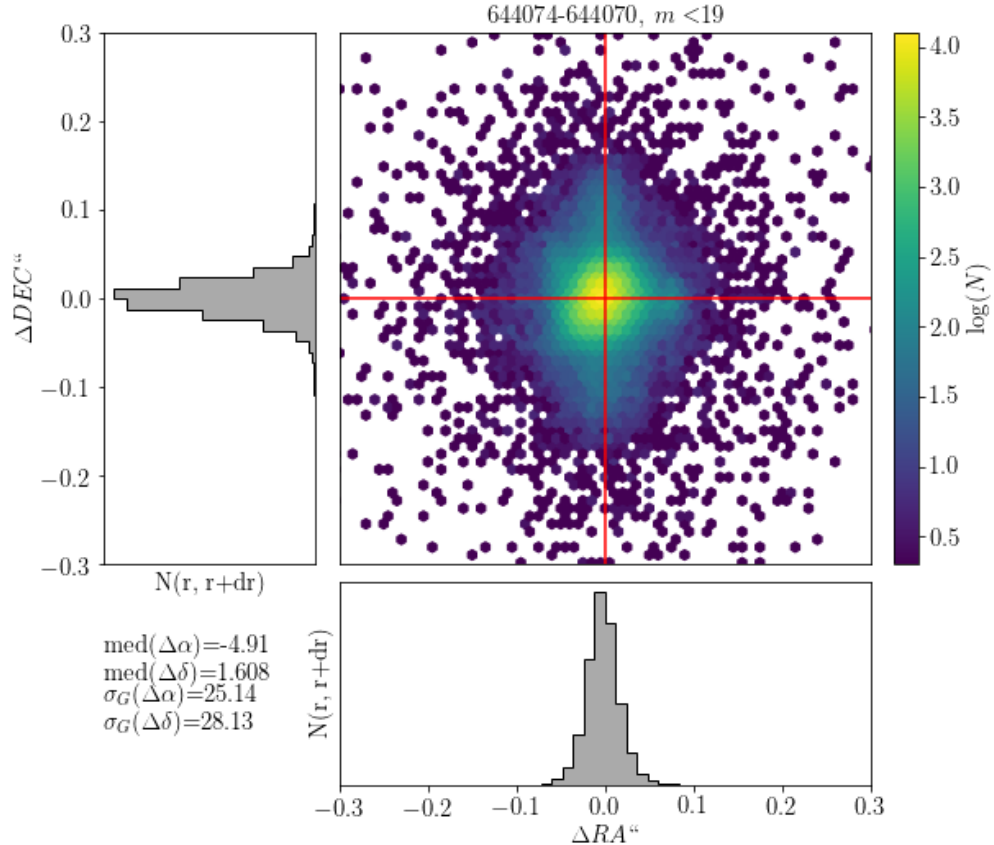


FIGURE 26: The difference in RA,DEC for the same visits as in Fig. 24, but comparing DECAPS single-epoch catalogs. The spread of  $\Delta\alpha$ ,  $\Delta\delta$  is wider than for equivalent visit pairs processed by the LSST Science Pipelines - see Table 10

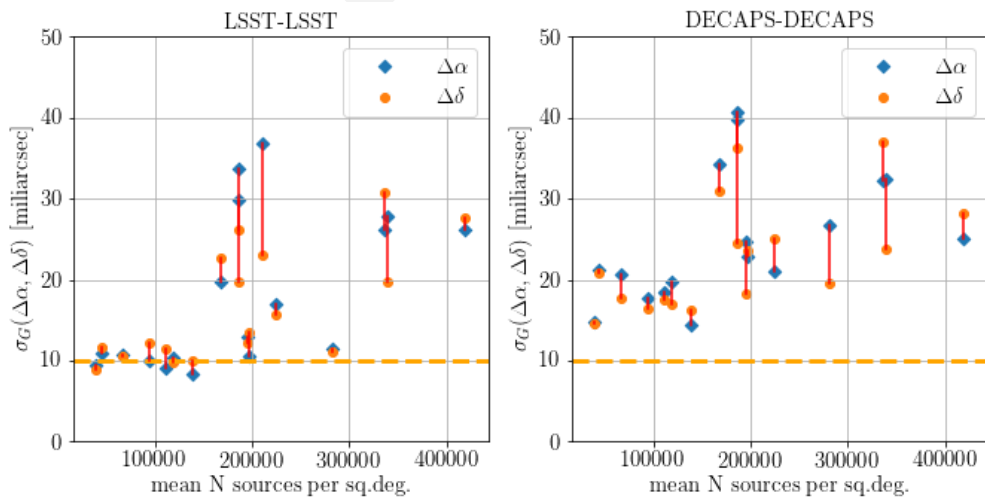


FIGURE 27: Summary of LSST and DECAPS repeatability of astrometry, as in Tables 9 and 10.

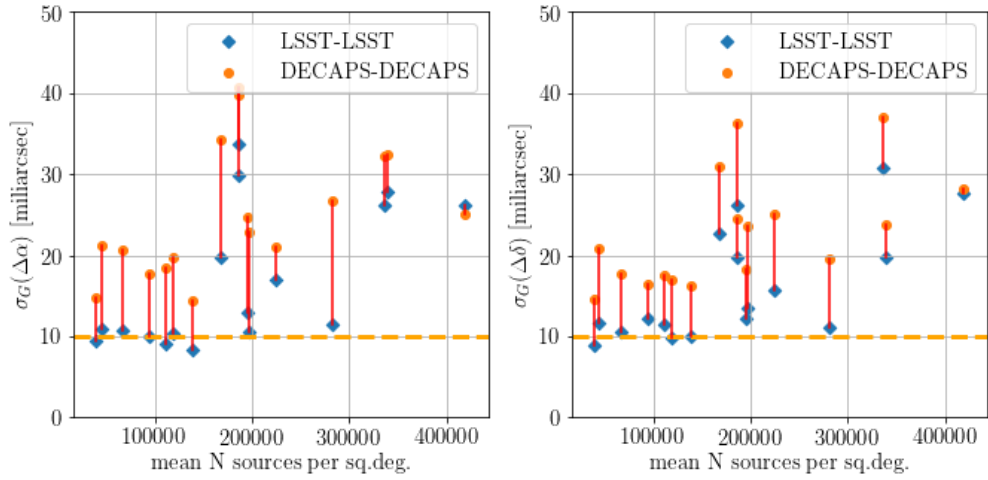


FIGURE 28: Comparison of LSST-LSST, DECAPS-DECAPS on the same scale, data from Tables 9 and 10.

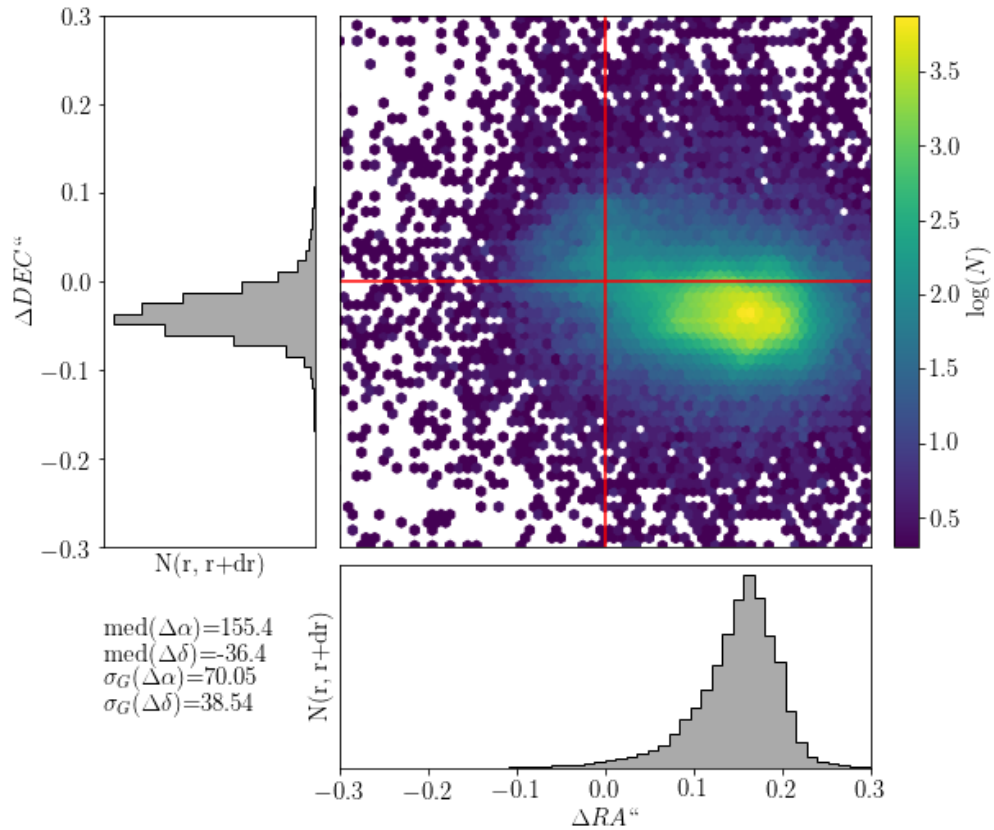


FIGURE 29: The difference in RA,DEC for visit 525904 , between LSST and DECAPS processing (402270 detected sources in the clean LSST catalog ). We tested that for other vists and in all cases the offset position and magnitude remains the same - see Table 11

TABLE 11: The difference in RA,DEC for the same visit analyzed by LSST and DECAPS. Each row corresponds to a separate visit, which correspond to different stellar density. All measured quantities are in miliarcseconds.

visit	median( $\Delta\alpha$ )	median( $\Delta\delta$ )	$\sigma_G(\Delta\alpha)$	$\sigma_G(\Delta\delta)$
525904	155.49	-36.46	70.06	38.55
525920	130.45	-27.53	72.83	43.88
525846	105.62	-51.71	42.49	30.04
525879	131.93	-42.62	138.58	75.68
525837	96.01	-47.93	65.17	36.6
525838	124.9	-68.92	59.56	33.99
525814	39.99	-29.87	47.26	29.72
525900	127.61	-32.38	54.81	33.67
527300	146.26	-38.73	56.49	25.48
527296	120.47	-26.98	41.65	27.14
530012	111.21	-51.38	35.01	28.34
530032	126.69	-47.85	115.02	65.23
527246	88.38	-49.06	45.87	30.6
527247	110.44	-66.18	43.15	29.71
529974	49.13	-30.91	48.55	28.95
529989	126.51	-33.77	52.12	28.33

## 7.1 LSST Processing of StarFast Simulated Sky

An independent way to further test the performance of the LSST Science Pipelines is to use the simulated sky images, where the true position and brightness of each source is known. This would put the measure of source detection completeness, photometric and astrometric precision on an absolute scale. We already tested a StarFast image simulator<sup>9</sup>, and confirmed that it can successfully simulate a region of the sky seeded with known stellar population.

## 7.2 Other LSST-DECAPS tests: w-color

An independent test of the quality of photometry would be to consider the width of the stellar locus ('w-color') on the g-r vs r-i color-color plot. This could be used to test internal consistency of LSST and DECAPS photometry.

<sup>9</sup><https://dmtn-012.lsst.io>

## References

- [1] Bosch, J., et al. 2017, ArXiv e-prints 1705.06766
- [2] Hogg, D. W. 2001, The Astronomical Journal, 121, 1207
- [3] Lupton, R. 2005, in prep.
- [4] Lupton, R., Gunn, J. E., Ivezić, Z., Knapp, G. R., & Kent, S. 2001, in Astronomical Society of the Pacific Conference Series, Vol. 238, Astronomical Data Analysis Software and Systems X, ed. F. R. Harnden, Jr., F. A. Primini, & H. E. Payne, 269
- [5] Lupton, R. H., Ivezić, Z., & Gunn, J. 2005, in prep.
- [6] Lupton, R. H., Ivezić, Z., Gunn, J. E., Knapp, G., Strauss, M. A., & Yasuda, N. 2002, in SPIE Proceedings, Vol. 4836, Survey and Other Telescope Technologies and Discoveries, ed. J. A. Tyson & S. Wolff, 350
- [7] Narayan, G., et al. 2018, ArXiv e-prints
- [8] Olsen, K. A. G., Blum, R. D., & Rigaut, F. 2003, AJ, 126, 452
- [9] Schlaflay, E. F., et al. 2017, ArXiv e-prints 1710.01309
- [10] Shaw, R. A. 2015, NOAO Data Handbook